Received: 14 April 2022 | Revised: 12 August 2022 | Accepted: 17 August 2022

DOI: 10.1002/glia.24265

GLIA

WILEY

RESEARCH ARTICLE

Reactive microglia are the major source of tumor necrosis factor alpha and contribute to astrocyte dysfunction and acute seizures in experimental temporal lobe epilepsy

Lukas Henning[1] | Henrike Antony[1] | Annika Breuer[1] | Julia Müller[1] | Gerald Seifert[1] | Etienne Audinat[2] | Parmveer Singh[3] | Frederic Brosseron[4] | Michael T. Heneka[5] | Christian Steinhäuser[1] | Peter Bedner[1]

[1]Institute of Cellular Neurosciences, Medical Faculty, University of Bonn, Bonn, Germany

[2]Institute of Functional Genomics, University of Montpellier, CNRS, INSERM, Montpellier, France

[3]Plexxikon Inc., Berkeley, California, USA

[4]German Center for Neurodegenerative Diseases (DZNE), Bonn, Germany

[5]Université du Luxembourg, Esch-sur-Alzette, Luxembourg

Correspondence
Christian Steinhäuser, Institute of Cellular Neurosciences, Medical Faculty, University of Bonn, Venusberg-Campus 1, 53105 Bonn, Germany.
Email: cste@uni-bonn.de

Funding information
BMBF, Grant/Award Numbers: 01DN20001, 16GW0182; EU, Grant/Award Number: H2020-MSCA-ITN

Abstract

Extensive microglia reactivity has been well described in human and experimental temporal lobe epilepsy (TLE). To date, however, it is not clear whether and based on which molecular mechanisms microglia contribute to the development and progression of focal epilepsy. Astroglial gap junction coupled networks play an important role in regulating neuronal activity and loss of interastrocytic coupling causally contributes to TLE. Here, we show in the unilateral intracortical kainate (KA) mouse model of TLE that reactive microglia are primary producers of tumor necrosis factor (TNF)α and contribute to astrocyte dysfunction and severity of *status epilepticus* (SE). Immunohistochemical analyses revealed pronounced and persistent microglia reactivity, which already started 4 h after KA-induced SE. Partial depletion of microglia using a colony stimulating factor 1 receptor inhibitor prevented early astrocyte uncoupling and attenuated the severity of SE, but increased the mortality of epileptic mice following surgery. Using microglia-specific inducible TNFα knockout mice we identified microglia as the major source of TNFα during early epileptogenesis. Importantly, microglia-specific TNFα knockout prevented SE-induced gap junction uncoupling in astrocytes. Continuous telemetric EEG recordings revealed that during the first 4 weeks after SE induction, microglial TNFα did not significantly contribute to spontaneous generalized seizure activity. Moreover, the absence of microglial TNFα did not affect the development of hippocampal sclerosis but attenuated gliosis. Taken together, these data implicate reactive microglia in astrocyte dysfunction and network hyperexcitability after an epileptogenic insult.

KEYWORDS
astrocyte, gap junction coupling, hippocampal sclerosis, microglia, temporal lobe epilepsy, tumor necrosis factor alpha

1 | INTRODUCTION

Accumulating clinical and experimental evidence indicates that neuroinflammation contributes to the pathophysiology of epilepsy (Aronica et al., 2017; Devinsky et al., 2013; Gershen et al., 2015; Löscher et al., 2020). Microglia are critical regulators of central nervous system (CNS) immunity and are highly reactive to various types of brain insults, including *status epilepticus* (SE), ischemia or infection (Eyo et al., 2014; Hanisch & Kettenmann, 2007; Qin et al., 2019; Rock et al., 2004). Importantly, there exist numerous reports of reactive microglia in both human and animal models of epilepsy (Broekaart et al., 2018; Feng et al., 2019; Hiragi et al., 2018; Morin-Brureau et al., 2018; Zattoni et al., 2011). In experimental temporal lobe epilepsy (TLE), microglia are characterized by an amoeboid morphology (De Simoni et al., 2000; Wyatt-Johnson et al., 2017), production of proinflammatory cytokines (Aronica et al., 2007; Benson et al., 2015; Sano et al., 2021; Varvel et al., 2016) as well as increased proliferation and enhanced K^+ conductance (Avignone et al., 2008; Feng et al., 2019). However, even though the link between reactive microglia and epilepsy is well documented, mechanistically the contribution of microglia to the pathophysiology of epilepsy is still incompletely understood.

A number of studies show that tumor necrosis factor alpha (TNFα) transcript and protein levels increase rapidly in brain parenchyma and microglia following SE (Benson et al., 2015; De Simoni et al., 2000; Lehtimäki et al., 2003; Nikolic et al., 2018; Sano et al., 2021; Vezzani et al., 2002). Moreover, TNFα signaling increases seizure susceptibility (Patel et al., 2017; Probert et al., 1995; Rana & Musto, 2018; Riazi et al., 2008; Weinberg et al., 2013). It remains unclear, however, whether microglia constitute the primary source of TNFα in experimental TLE, as other cells including astrocytes and infiltrating monocytes, are also immunocompetent (Devinsky et al., 2013; Vezzani et al., 2011). Previously, we have shown that disruption of astrocytic gap junction (GJ) coupling and concomitant impairments in extracellular K^+ buffering temporally precede neuronal cell death and spontaneous seizure development in a mouse model of kainate (KA)-induced TLE, pointing to a causal involvement in the genesis of the disease (Bedner et al., 2015). The seizure-induced decrease in coupling could be mimicked *in situ* by incubation of acute hippocampal slices with a combination of interleukin 1ß (IL1ß) and TNFα (Bedner et al., 2015). Similarly, both treatment of cultured primary astrocytes with TNFα as well as co-culturing of astrocytes with activated microglia impair coupling efficiency (Haghikia et al., 2008; Même et al., 2006). Together, these data suggest that microglial cytokines indirectly promote epileptogenesis, by reducing coupling efficiency and thus the K^+ and glutamate buffering capacity of astrocytes. In the present study, we therefore examined the contribution of reactive microglia and microglial TNFα to astrocyte GJ uncoupling and epileptogenesis in a mouse model of TLE. Pharmacological depletion of microglia using the colony-stimulating factor 1 receptor (CSF1R) inhibitor PLX5622 combined with microglia-specific inducible knockout of TNFα were employed to assess the contribution of microglia to early astrocyte dysfunction and TNFα production following KA-induced SE. Additionally, continuous telemetric electroencephalography (EEG) was combined with immunohistochemistry to investigate effects of TNFα depletion in microglia on acute and chronic epileptiform activity as well as the development of hippocampal sclerosis (HS).

2 | MATERIALS AND METHODS

2.1 | Animals

Male C57B6/J, FVB (Charles River, Sulzfeld, Germany) or GFAP-eGFP (Nolte et al., 2001) mice aged 90–120 days were used for the experiments. To study the effects of microglia specific knock-out of TNFα on epileptogenesis and astrocytic gap junction coupling, $Cx3cr1^{CreERT2}$ knock-in mice (Yona et al., 2013) were crossed with $TNF\alpha^{loxp/loxp}$ (Grivennikov et al., 2005) mice to yield $Cx3cr1^{CreERT2/+}$-$TNF\alpha^{loxp/loxp}$ mice. Both male and female $Cx3cr1^{CreERT2/+}$-$TNF\alpha^{loxp/loxp}$ and $Cx3cr1^{CreERT2/+}$-$TNF\alpha^{+/+}$ were used. Maintenance and handling of animals were performed according to EU and local governmental regulations. Experiments were approved by the North Rhine–Westphalia State Agency for Nature, Environment and Consumer Protection (approval number 84-02.04.2015.A393 and 81-02.04.2020.A420). All measures were taken to minimize the number of animals. Mice were kept under standard housing conditions (12 h/12 h dark–light cycle) with food and water provided *ad libitum*.

2.2 | Drugs

2.2.1 | Tamoxifen treatment

To induce site-specific recombination of loxP-flanked sequences, $Cx3cr1^{CreERT2/+}$-$TNF\alpha^{loxP/loxP}$ and $Cx3cr1^{CreERT2/+}$-$TNF\alpha^{+/+}$ mice received intraperitoneal (i.p.) injections of tamoxifen (Sigma-Aldrich, #T5648, Steinheim, Germany) dissolved in sunflower seed oil (Sigma-Aldrich, #88921) and EtOH at a ratio of 1:10. Mice were injected daily for 5 consecutive days receiving 2 mg per day of tamoxifen (100 µl per mouse). A comparable treatment regimen has previously been shown to induce high site-specific recombination in the CNS of this Cre-mouse line (Goldmann et al., 2013). Mice were used for experiments ~30 days after tamoxifen administration in order to restrict Cre-mediated recombination to microglia (Parkhurst et al., 2013). Tamoxifen-injected $Cx3cr1^{CreERT2/+}$-$TNF\alpha^{+/+}$ mice served as the control group (CTRL).

2.2.2 | PLX5622 treatment

PLX5622 was provided by Plexxikon Inc. (Berkeley, CA 94710, USA) and formulated in AIN-76A standard chow by Research Diets Inc. (New Brunswick, NJ 08901 USA) at 1200 ppm. Male FVB or C57B6J mice were fed with either a PLX5622-containing or AIN-76A control

diet for 7, 21, or 28 consecutive days before the start of the experiments. Twenty-one days of oral PLX5622 application have previously been shown to almost completely deplete IBA1$^+$ microglia from the brain (Dagher et al., 2015). The diet was provided *ad libitum* and food intake was monitored by weighing the amount of diet consumed by the animals.

2.3 | Unilateral intracortical kainate injection and implantation of telemetric EEG transmitters

We employed the TLE-HS animal model as described previously (Bedner et al., 2015; Deshpande et al., 2020; Henning et al., 2021). Briefly, mice were anesthetized with a mixture of medetomidine (Cepetor, CP-Pharma, Burgdorf, Germany, 0.3 mg/kg, i.p.) and ketamine (Ketamidor, WDT, Garbsen, Germany, 40 mg/kg, i.p.) and placed into a stereotaxic frame equipped with a manual microinjection unit (David Kopf; Tujunga, CA, USA). A total volume of 70 nl of a 20 mM solution of KA (Tocris, Bristol, UK) dissolved in 0.9% sterile NaCl was stereotaxically injected into the neocortex just above the right dorsal hippocampus. The stereotaxic coordinates were: 2 mm posterior to bregma, 1.5 mm from midline, and 1.7 mm from the skull surface. Sham control mice received injections of 70 nl saline under the same conditions. Immediately after KA injection, two drill holes were made at 1 mm posterior to the injection site and 1.5 mm lateral from midline to insert two monopolar leads required for electrographic seizure detection. Telemetric transmitters (TA10EA-F20 or TA11ETA-F10; Data Sciences International (DSI), St. Paul, MN, USA) were implanted subcutaneously into the right abdominal region and the two monopolar leads were inserted ~1 mm deep into the cortex. Attached leads were fixed to the skull using superglue and covered with dental cement. The scalp incision was subsequently sutured and anesthesia stopped with atipamezol (Antisedan, Orion Pharma, Hamburg, Germany, 300 mg/kg, i.p.). To reduce pain, mice were injected with carprofen for 3 days (Rimadyl, Pfizer, Karlsruhe, Germany). Moreover, 0.25% Enrofloxacin (Baytril, Bayer, Leverkusen, Germany) was administered via drinking water to reduce the risk of infection. After surgery, mice were returned to clean cages and placed on individual radio receiving plates (RPC-1; Data Sciences International, New Brighton, MN, USA), which capture data signals from the transmitter and send them to a computer running Ponemah software (Version 5.2, Data Sciences International). EEG recordings (24 h/day, 7 days/week) were started directly after transmitter implantation and continued for 28 days after SE induction.

2.4 | EEG data analysis

EEG data was analyzed using NeuroScore (version 3.4.0) software (Data Sciences International) as described previously (Henning et al., 2021). Briefly, recordings were high pass filtered at 1 Hz and the number of seizures, their duration and spike numbers were determined using the spike train analysis tool implemented in NeuroScore based on the following criteria: threshold value = 7.5 × SD of the baseline (i.e., activity during artifact- and epileptiform-free epochs four weeks after SE) − 1000 μV, spike duration = 0.1–50 ms, spike interval = 0.1–2.5 s, minimum train duration = 30 s, train join interval = 1 s, minimum number of spikes = 50. The number of artifacts was minimized by repeating the spike train analysis with a threshold ranging from the maximum amplitude of actual epileptiform spikes (i.e., determined subjectively by manually scrolling through the EEG recording) − 1000 μV and subsequently subtracting that value from the value obtained during initial spike quantification (i.e., 7.5 × SD of the baseline − 1000 μV). Fast Fourier transformation (FFT) was conducted to derive absolute δ (0.5–4 Hz), θ (4–8 Hz), α (8–13 Hz), β (13–30), and γ (30–50 Hz) power values, which were normalized to baseline activity prior to conducting statistics. The number of spontaneous generalized seizures during the chronic phase was determined manually from the EEG recordings by two experienced experimenters. Finally, to analyze EEG activity during SE in PLX5622 treated mice, spike number and EEG band power were normalized to the activity during the postictal state. For that, activity during at least five postictal periods lasting ~10 s was quantified. The spike threshold was set at 10 × SD of baseline activity during the postictal state. All animals included in the study developed SE. Three animals (2 PLX and 1 control mice) were excluded from the analysis because the EEG signal was too noisy to allow accurate quantification of the baseline EEG activity.

2.5 | Whole-cell patch clamp and biocytin-filling of astrocytes

Mice were anesthetized with isoflurane (Piramal Healthcare, Morpeth, UK) and decapitated. Brains were quickly removed and 200 μm-thick coronal slices were cut on a vibratome (VT1000S, Leica Microsystems, Wetzlar, Germany) in ice cold preparation solution containing (in mM): 87 NaCl, 2.5 KCl, 1.25 NaH_2PO_4, 25 $NaHCO_3$, 7 $MgCl_2$, 0.5 $CaCl_2$, 25 glucose, 75 sucrose, equilibrated with carbogen to stabilize pH (5% CO_2/95% O_2, pH 7.4). After storage of slices (15 min, 35°C) in preparation solution, slices were transferred to a solution containing (in mM): 126 NaCl, 3 KCl, 2 $MgSO_4$, 2 $CaCl_2$, 10 glucose, 1.25 NaH_2PO_4, 26 $NaHCO_3$, gassed with carbogen (aCSF). To aid identification of astrocytes in the tissue, aCSF was supplemented with SR101 (1 μM, Sigma Aldrich, S7635, incubation 20 min, 35°C) (Kafitz et al., 2008). After SR101 staining, slices were transferred to aCSF and kept at room temperature (RT) for the duration of the experiments. For recordings, slices were transferred to a recording chamber and constantly perfused with aCSF. Patch pipettes fabricated from borosilicate capillaries with a resistance of 3–6 MΩ were filled with a solution containing (in mM): 130 K-gluconate, 1 $MgCl_2$, 3 Na_2-ATP, 20 HEPES, 10 EGTA and biocytin (0.5%, Sigma Aldrich) (pH 7.2, 280–285 mOsm). To analyze gap junction coupling, whole-cell patch clamp recordings of SR101-positive astrocytes were performed during which astrocytes were filled with biocytin (20 min, RT). In addition to SR101 staining, astrocytes were identified by their characteristic morphology,

passive current–voltage relationship, low input resistance and a resting membrane potential close to the Nernst potential of K^+. Current signals were amplified (EPC 8, HEKA Electronic, Lambrecht, Germany), filtered at 3 or 10 kHz, and sampled at 10 or 30 kHz (holding potential −80 mV). Online analysis was performed with TIDA 5.25 acquisition and analysis software for Windows (HEKA) and Igor Pro 6.37 software (WaveMetrics, Lake Oswego, OR, USA). Voltages were corrected for liquid junction potentials. Only recordings matching the following criteria were included in the analysis: (i) resting potential negative to −60 mV, (ii) membrane resistance ≤10 MΩ, and (iii) series resistance ≤20 MΩ. After the recording, slices containing a biocytin-filled astrocyte were stored in 4% paraformaldehyde (PFA)-containing phosphate buffered saline (PBS) overnight at 4°C and subsequently transferred into PBS and stored at 4°C until immunohistochemistry.

2.6 | Immunohistochemistry

2.6.1 | Tissue preparation

Animals were deeply anaesthetized by i.p. injection with 100–120 µl of a solution containing 40 mg/kg ketamine (WDT) and 0.3 mg/kg, medetomidine (CP-Pharma). After checking for hind paw reflexes, transcardial perfusion was applied with ice-cold PBS (30 ml) followed by 4% ice-cold PFA in PBS (30 ml). Brains were removed and stored for 24–48 h in 4% PFA-containing solution and subsequently stored in PBS at 4°C until slicing. Brains were cut into 40 µm thick coronal slices using a Leica VT1200S vibratome (Leica Microsystems).

2.6.2 | Antibody staining

Immunohistochemistry was performed using free-floating slices kept in 24-well plates. Slices from the dorsal hippocampus close to the KA injection site were used. For membrane permeabilization and blocking of unspecific epitopes, slices were incubated (1–2 h, RT) with 0.5% Triton X-100 (or 2% for staining of biocytin-filled astrocytes) and 10% normal goat or donkey serum (NGS, NDS) in PBS. Slices were subsequently incubated overnight with primary antibody solution containing PBS on a shaker at 4°C. The following primary antibodies were applied: rat anti-CD68 (1:200, BioRad Laboratories, MCA1957, Munich, Germany), rat anti-CD169 (1:400, BioRad Laboratories, MCA884), rabbit anti-GFAP (1:500, DAKO, Z0334, Hamburg, Germany), rabbit anti-IBA1 (1:400, Wako Chemicals, #019-19741, Neuss, Germany), mouse anti-NeuN (1:200, Merck Millipore, MAB377, Darmstadt, Germany), rabbit anti-Tmem119 (1:500, Abcam, ab209064), rabbit anti-TNFR1 (1:100, Abcam, ab19139, Berlin, Germany). On the following day, slices were washed three times with PBS for 5–10 min each and subsequently incubated with secondary antibodies conjugated with Alexa Fluor® 488, Alexa Fluor® 647, streptavidin-conjugated Alexa Fluor® 647 (1:500, 1:600 respectively, Invitrogen, Karlsruhe, Germany) or streptavidin-conjugated Cy3 antibody (1:300, Sigma Aldrich, S6402) in PBS (2% NGS, 1.5-2 h, RT). For staining of NeuN, slices were incubated with goat anti-mouse biotin (1:500, Dianova, AB_2338557, Hamburg, Germany) prior to incubation with streptavidin-conjugated Cy3 antibody (1 h, RT). After washing slices again three times with PBS (5–10 min), nuclear staining with Hoechst (1:200, diluted in dH_2O) was performed (10 min, RT). A final washing step (3× PBS, 5 min each) was performed and slices were mounted with Aquapolymount (Polysciences, Heidelberg, Germany) on objective slides and covered with cover slips. Slides were stored at 4°C before confocal imaging.

2.6.3 | Confocal microscopy

A confocal laser scanning microscope (SP8, Leica, Hamburg, Germany) at 8 bit using 10× (numerical aperture (NA): 0.4) 20× (NA: 0.75), 40× (NA: 1.1), and 63× (NA: 1.2) objectives was used. Image resolution was set at 1024 × 1024 pixels recorded at a speed of 400 Hz, with a pinhole size of 1 airy unit (AU). Standard photomultiplier tubes or hybrid detectors were used for detection of fluorescent signals. Laser and detector settings were applied equally to all images acquired. Z-stacks were recorded at 0.36 µm (TNFR1), 0.42 µm (CD68), 1 µm (IBA1 & GFAP morphology, CD169), or 2 µm (GJ coupling & Hippocampal sclerosis) intervals.

2.7 | Quantification of immunostainings

2.7.1 | Microglial/macrophage morphology

Microglia/macrophage morphology was quantified based on IBA1 staining using the publicly available (https://github.com/hansenjn/MotiQ) plugin MotiQ for FIJI (Schindelin et al., 2012). Two to four $IBA1^+$ cells per image were cropped out of 30 µm z-stacks (40×/1.1 NA objective, region of interest (ROI): 242.42 × 242.42 × 30 μm^3) from each condition to create single-cell images. Next, single-cell images were binarized by application of an automated intensity threshold (Otsu for KA experiments and Moments for PLX5622 experiments) to 0.5 scaled maximum intensity projections (MIPs) of the original image. Binary single-cell images were further filtered by removing all particles smaller than 100 voxels from the image. Finally, 3D reconstructions and skeletons were generated from which cell volume, average and total process length, ramification and polarity index were quantified and statistically compared between conditions. A Gauss filter (sigma = 2) was applied prior to skeletonization. The ramification index indicates the complexity of the cell's shape using the following equation:

$$\text{Ramification index} = \frac{\text{cell surface area}}{4\pi \times \left(\frac{3 \times \text{cell volume}}{4\pi}\right)^{\frac{2}{3}}} \quad (1)$$

The polarity index was defined as:

$$\text{Polarity index} = \frac{\text{convex hull center} - \text{cell center}}{2 \times \sqrt[3]{\frac{3 \times \text{convex hull volume}}{4\pi}}} \quad (2)$$

and indicates the degree of unbalance in the distribution of processes emanating from the cell's soma (Fülle et al., 2018). The density of IBA1$^+$ and CD169$^+$ (ROI: 242.42 × 242.42 × 30–32 μm^3) cells was quantified using the spot detection algorithm implemented in IMARIS 8.0 (Bitplane, Zurich, Switzerland).

2.7.2 | Microglia and astrocyte morphology and marker expression in PLX5622 experiments

The number of IBA1$^+$ cells as well as the total volume occupied by the microglia-specific marker Tmem119 in PLX5622-treated FVB mice were determined in 3D images recorded using either a 10×/0.4 NA objective (IBA1; ROI: 969.70 × 969.70 × 15 μm^3) or 40×/1.1 NA objective (Tmem119; ROI: 242.42 × 242.42 × 15–17 μm^3) using the spot and surface detection algorithms implemented in IMARIS 8.0, respectively. Moreover, astrocyte morphology was determined based on GFAP staining in 3D images (63×/1.2 NA objective; ROI: 153.92 × 153.92 x 30 μm^3) using the in-built Autopath algorithm implemented in IMARIS 8.0. Reconstruction parameters were kept identical across all images analyzed.

2.7.3 | Quantification of CD68 and IBA1 volumes

Custom-written macros in FIJI were used to determine the volume of CD68 and IBA1 signals occupied in each image (40×/1.1 NA objective; ROI: 242.42 × 242.42 × 20–22 μm^3). Images were background subtracted (15 pixel rolling ball radius), median filtered (2 pixel radius) and subsequently binarized (Triangle for CD68 and Moments threshold for IBA1) after which the area occupied by the respective signal within each focal plane was quantified using the analyze particles function in FIJI. The obtained area values were subsequently summed up across all focal planes in order to obtain the total volume occupied by each signal.

2.7.4 | Colocalization of TNFR1 and GFAP

Colocalization analysis was performed with FIJI in TNFR1/GFAP double-stained hippocampal sections of KA-injected or control C57B6J mice. Images were recorded using a 63×/1.2 NA objective (ROI: 92.35 × 92.35 × 12 μm^3). GFAP$^+$ images were median filtered (3 pixel radius) and subsequently binarized (Triangle threshold). Image values of 0 and 1 were obtained by subtraction of the value 254 from the thresholded GFAP$^+$ image. Next, the binary GFAP$^+$ images and the TNFR1$^+$ images were multiplied to derive the TNFR1 signal intensity in GFAP$^+$ pixels. Signal intensities were subsequently summed up across all focal planes to derive the total TNFR1 content in astrocytes. Cumulative TNFR1 signal intensity was divided by the total volume occupied by the GFAP signal to account for differences in GFAP expression between experimental conditions.

2.7.5 | Coupling efficiency of biocytin-filled astrocytes

Coupling efficiency was determined by manual counting of biocytin$^+$ cells using the cell counter plugin implemented in FIJI and compared between injected (ipsilateral) and non-injected (contralateral) hemispheres. Another observer blinded to the experimental conditions recounted images of biocytin-filled astrocytes, and cell counts were subsequently averaged across both counts prior to statistical analysis.

2.7.6 | Hippocampal sclerosis

The extent of hippocampal sclerosis was estimated based on the quantification of four parameters: (i) the extent of granule cell dispersion (GCD) in the dentate gyrus (DG), (ii) the shrinkage of the CA1 *stratum radiatum*, (iii) the number of CA1 pyramidal neurons, and (iv) the extent of astrogliosis in CA1 *stratum radiatum*. GCD, *stratum radiatum* shrinkage and the number of CA1 pyramidal neurons were estimated in maximum intensity projections (MIPs) (ROI: 1163.64 × 1163.64 × 30–32 μm^3). The extent of astrogliosis was measured in individually defined ROIs in CA1 *stratum radiatum* and subsequently normalized to ROI size. GCD quantification was performed as described previously (Deshpande et al., 2020; Henning et al., 2021). Briefly, GCL width was measured at four positions indicated as T1–T4. T1 and T2 were measured along a vertical line connecting the upper and lower cell layers of the DG, T3 and T4 at a distance halfway between the vertical line and the tip of the hilus. The average of the four values was used as an estimation of GCD. Shrinkage of the *stratum radiatum* was determined by drawing a vertical line connecting the pyramidal and molecular layer, above the highest point of the DG granule cell layer. The length of the vertical line served as an indication of the remaining width of the *stratum radiatum*. The extent of astrogliosis was measured by quantifying the area occupied by the GFAP signal in individual ROIs within all focal planes of each image. The total volume occupied by the GFAP signal was subsequently derived by summing up the area calculated across all focal planes and was normalized to the volume of the ROI prior to statistical analysis. Both GCD, *stratum radiatum* width and astrogliosis were quantified using FIJI software. The number of pyramidal neurons in the CA1 region was measured using the automated spot detection algorithm implemented in IMARIS8.0 within a 360 × 120 × 30 μm^3 ROI placed within the CA1 pyramidal layer just above the highest point of the DG granule cell layer.

2.8 | Quantification of hippocampal TNFα concentrations

2.8.1 | Tissue preparation and biochemical extraction of hippocampal protein

$Cx3cr1^{CreERT2/+}$-$TNF\alpha^{loxp/loxp}$ and $Cx3cr1^{CreERT2/+}$-$TNF\alpha^{+/+}$ mice were transcardially perfused as described above. Dorsal hippocampi were quickly removed, weighed and flash frozen in liquid nitrogen before storage at −80°C until biochemical extraction. Frozen hippocampi were homogenized in homogenization buffer (1× PBS, 5 mM NaF, 20 mM pyrophosphate, 1× protease/phosphatase inhibitor (Cell Signaling, #5872, Frankfurt am Main, Germany)) using a Precellys® device (Bertin Instruments, Darmstadt, Germany) for 2× 15 s at 5000 rpm. Next, an equal volume of 2× RIPA buffer (50 mM Tris, 150 mM NaCl, 2% NP-40, 1% NaDOC, 0.2% SDS) was added to the sample, followed by sonication of the sample for 10 s and incubation on ice for 30 min. The homogenate was centrifuged for 30 min at 100,000*g* and the supernatant was collected. The total protein concentration in the supernatants was determined using a bicinchoninic acid (BCA) assay (Thermo Fisher Scientific, Bremen, Germany) according to the manufacturer's instructions.

2.8.2 | ELISA

For quantification of hippocampal TNFα concentrations an electrochemiluminescence ELISA (V-PLEX Mouse TNF-α Kit, K152QWD, MESO SCALE DIAGNOSTICS, LLC, Rockville, USA) was performed with a 1:1 sample dilution using the reagents supplied by the manufacturer and according to the manufacturer's instructions. Each sample was measured in duplicate and the average was normalized to the weight of hippocampal tissue and expressed as pg/mg tissue.

2.9 | Single-cell semiquantitative real time reverse transcription PCR

Single-cell transcript analysis was performed on astrocytes harvested from brain slices of the hippocampal CA1 region of KA-injected and non-injected C57B6J mice (Seifert et al., 2009). Astrocytes were identified by labeling with the fluorescent dye SR101 and based on electrophysiological characterization. Cells were aspirated into a patch pipette and expelled into reaction tubes filled with 3 µl DEPC-treated water, flash frozen in liquid nitrogen and stored at −20°C until the start of the RT-PCR. A reverse transcription reaction was started by adding 4.5 µl RT-mastermix containing RT-buffer (ThermoScientific), dNTPs (4 × 250 µM, ThermoFisher), random hexamers (50 µM, Roche) RNasin (20 U, Promega), and Maxima H Minus reverse transcriptase (100 U, ThermoScientific) and incubated at 37°C for 1 h. Next, 40 µl of the mastermix were added to the RT product and a preamplification was performed for 20 cycles (denaturation at 94°C, 25 s; annealing at 51°C, 45 s; extension at 72°C, 25 s; final elongation at 72°C, 7 min) with a thermocycler PTC-200 (MJ Research). The mastermix contained PCR buffer, $MgCl_2$ (2.5 mM), dNTPs (4 × 50 µM), primers (200 nM each, Eurogentec), and 5 U Taq polymerase (Invitrogen). Thereafter, an aliquot of 1 µl was used as template for the real-time PCR using Takyon Mastermix (Eurogentec) or TaqMan universal PCR Mastermix for amplification of TNFα (Applied Biosystems), in a final volume of 12.5 µl. For detection and quantification of TNFR1, TNFR2, TNFα, and the reference genes GFAP and HPRT1, a Taqman primer/probe mix was used (Applied Biosystems). PCRs for the respective target and housekeeping genes were run in parallel wells for each sample as triplicates using a CFX384 Touch Real-Time PCR Detection System (BioRad Laboratories). Samples were incubated for 2 min at 50°C and after denaturation (10 min, 95°C), 50 cycles (denaturation at 95°C, 15 s; primer annealing and extension at 60°C, 60 s) were performed. The accumulation of the PCR product was detected by consecutively measuring the fluorescence intensity of the Taqman probe during each PCR cycle. The target gene/GFAP and target gene/HPRT1 expression ratios were determined by comparing C_T values of the target gene with those of the respective reference genes. The relative quantification of different genes was determined according to the following equation:

$$X_{\text{target}}/X_{\text{GFAP/HPRT1}} = E_{\text{GFAP/HPRT1}}^{\text{CT GFAP/HPRT1}}/E_{\text{target}}^{\text{CT target}} \quad (3)$$

yielding the gene ratio with X being the input copy number, E is the efficiency of amplification, and C_T is the cycle number at threshold detection. By quantification of target gene expression relative to GFAP or HPRT1, C_T was determined for each gene at the same fluorescence emission, R_n. The amplification efficiency was determined based on serial dilutions of mRNA and was 2.08 (HPRT1), 1.98 (GFAP), 2.03 (TNFR1), 2.02 (TNFR2), and 1.94 (TNFα). DEPC-water added to the RT-reaction served as a negative control.

2.10 | Statistical analysis

All statistical analyses were performed using R software (R Core Team, 2021, version 4.0.5, Austria) (R Core Team, 2021). Data are displayed as mean + standard deviation (SD) or as box plots representing median (line) and quartiles (25th and 75th percentile) with whiskers extending to the highest and lowest values within 1.5 times the interquartile range (IQR). Prior to statistical analysis, data were checked for normality by inspection of histograms and Q–Q plots as well as by applying a Shapiro–Wilk test. Levene's test was performed to check for homogeneity of variance between groups. In case of a significant deviation from normality, data were transformed according to Tukey's ladder of powers (Tukey, 1977) prior to conduction of statistical tests or by performing the appropriate non-parametric equivalent. For comparison of two independent groups, Student's *t*-test or Wilcoxon-rank sum test were used. More than two groups were compared with one-way analysis of variance (ANOVA) followed by post-hoc Tukey test or using Kruskal–Wallis test with Dunn's post-hoc test. *p*-Value

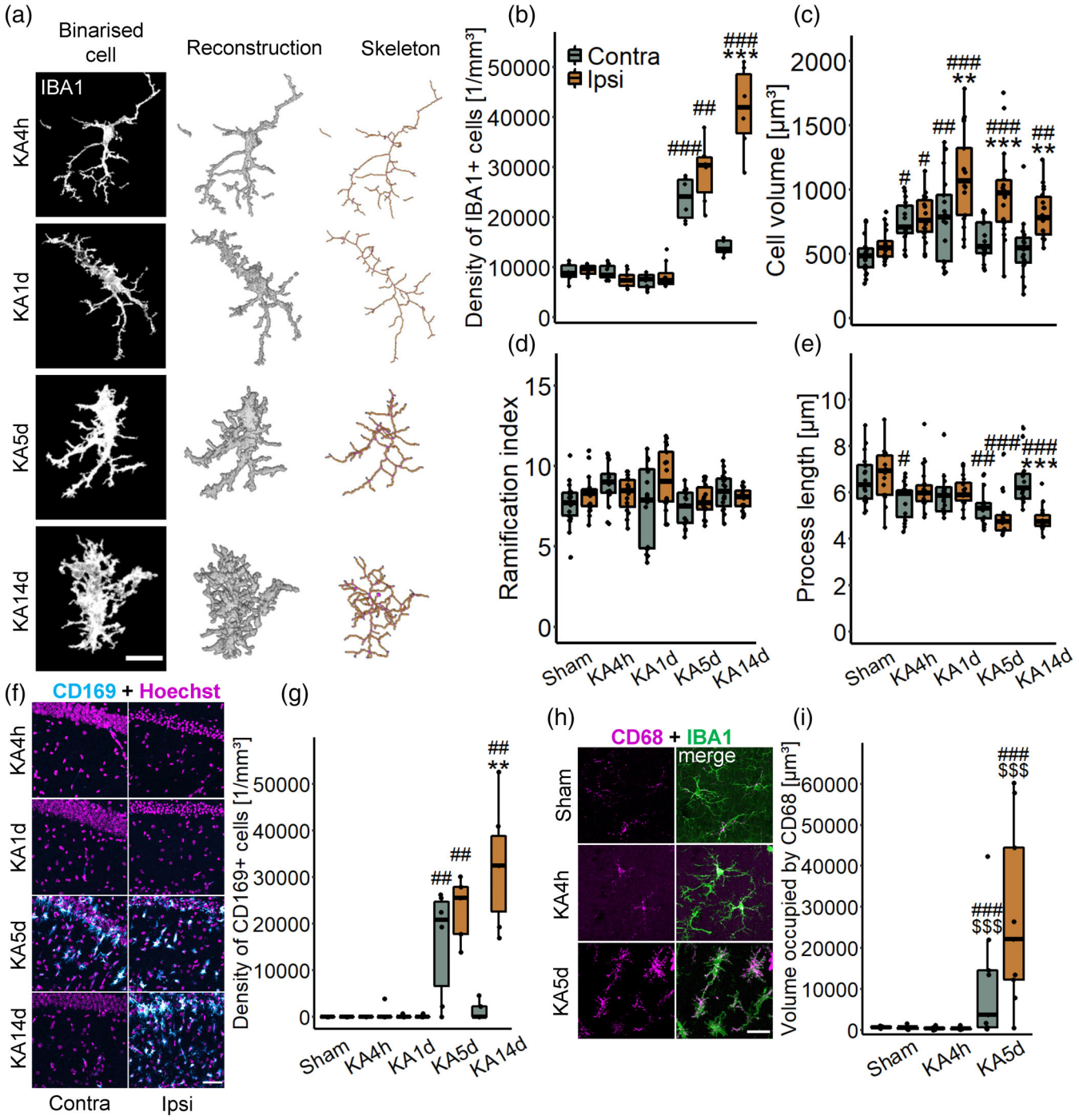

FIGURE 1 KA-induced TLE induces rapid microglia reactivity accompanied by delayed macrophage infiltration. (a) Representative images depicting the morphology of individual IBA1-positive cells in the ipsilateral hippocampal CA1 *stratum radiatum* of FVB mice at 4 h, 1, 5, and 14 days post SE induction. 3D reconstructions and skeletons were derived from the images to quantify the morphology of individual microglia/macrophages. Scale bar: 10 µm. (b–e) Quantitative analyses of density, volume, ramification index, and average process length of IBA1-positive cells indicate rapid and persistent activation of microglia/macrophages following KA-induced SE. $n = 15–20$ cells/condition, $N = 3$ mice/condition; two-way ANOVA; * versus contra, # versus sham. (f) Representative maximum intensity projection (MIPs) of CD169-positive macrophages (cyan) at 4 h, 5 days, and 14 days post SE induction. Scale bar: 50 µm. Images are background subtracted and brightness adjusted. (g) CD169 expression was increased in the hippocampal CA1 *stratum radiatum* during the latent and chronic periods, but not during SE. $n = 2–3$ slices/mouse, $N = 3$ mice/condition; two-way ANOVA; * versus contra, # versus sham. (h) Representative MIPs of a combined CD68 (magenta) and IBA1 (green) staining in the ipsilateral hippocampal CA1 *stratum radiatum* of sham- and KA-injected mice. Scale bar: 20 µm. Images depict a background subtracted and brightness adjusted region of interest (ROI) representative of the whole image. (i) CD68 expression was increased during the latent phase after KA-induced SE. $n = 3$ slices/mouse, $N = 3$ mice/condition; two-way ANOVA; # versus sham, $ versus KA4h. Data are displayed as box plots representing median and quartiles. Black dots represent individual data points. $^{**}p < 0.01$, $^{***}p < 0.001$; $\#p < 0.05$, $\#\#p < 0.01$, $\#\#\#p < 0.001$, $\$\$\$p < 0.001$

adjustment for more than two groups was based either on Tukey's or the Benjamini–Hochberg method. For multifactorial data, two-way ANOVA or two-way aligned rank transform ANOVA (Wobbrock et al., 2011) were performed. Kaplan–Meier estimates were compared using a log-rank test and Fisher's exact test was used to analyze contingency tables. Differences between groups were considered statistically significant at $p < 0.05$. If not stated otherwise, "*n*" refers to the number of cells or slices, and "*N*" refers to the number of animals used.

3 | RESULTS

3.1 | Activation of innate immune cells in experimental TLE

Activation of microglial cells and invasion of neural tissue by blood-derived immune cells has been described in the sclerotic hippocampus of drug-resistant TLE patients and in various experimental epilepsy models (Broekaart et al., 2018; Di Nunzio et al., 2021; Feng et al., 2019; Morin-Brureau et al., 2018; Zattoni et al., 2011). In the unilateral intracortical KA mouse model of TLE with HS, which closely reproduces key features of the human condition, pronounced microgliosis was found in the chronically epileptic hippocampus (Deshpande et al., 2020). However, the time course of microglial activation during the early phase of epileptogenesis has not been studied in our model, and no information on immune cell infiltration is yet available. Here, we performed morphometric analysis of IBA1-immunolabeled cells in the hippocampal CA1 at different stages of KA-induced epileptogenesis to assess the temporal pattern of microglia activation. We focused on four different time points, representing the acute phase (i.e., before onset of neuronal death, 4 h post KA injection), the latent period (1 and 5 days) and the chronic phase (14 days) (Bedner et al., 2015). Microglial cell density, cell volume, branching index and average length of cell processes were quantified using 3D reconstructions and cytoskeletal predictions extracted from high-resolution confocal images (Figure 1a) and statistically compared between sham- and KA-injected mice as well as between the injected (ipsilateral) and non-injected (contralateral) hemispheres. The density of IBA1-positive cells remained unchanged 4 h and 1 day after KA injection, but increased markedly on the fifth day in the hippocampi of both hemispheres. While after two weeks innate immune cell density further increased on the ipsilateral side, it returned to baseline contralaterally (Figure 1b, see Table S2 for descriptive statistics of Figure 1). Hypertrophy of IBA1-positive cells was already detectable 4 h after KA injection (Figure 1c). Similar to the alterations in cell density, these changes, as well the reduction in process length (Figure 1e), were persistent ipsilaterally but transient on the contralateral side. However, ramification of IBA1-positive cells remained unchanged across all time points investigated (Figure 1d).

As not only microglia but also peripheral monocytes express IBA1, we next sought to determine to what extent the increased density of IBA1-positive cells resulted from microglial proliferation vs. invasion of monocytes. For this purpose, we stained hippocampal slices from epileptic mice with the peripheral myeloid marker CD169 (Butovsky et al., 2012; Gao et al., 2015; Rice et al., 2015). CD169-positive cells were virtually absent 4 h and 1 day after KA, but abundant on both hemispheres after 5 days, and ipsilaterally after 14 days (Figure 1f,g). In order to test that in our model CD169 specifically labels peripheral monocytes, we performed double-staining of CD169 together with the microglia-specific marker Tmem119 (Bennett et al., 2016) 5 days post KA injection (Figure S1). Surprisingly, the staining revealed that a subset of CD169-positive cells also expressed Tmem119. Ipsilaterally, however, some CD169-positive cells were Tmem119-negative, which indicates monocyte infiltration.

To further characterize innate immune cell activation, we performed immunohistochemical staining for CD68, which is typically upregulated during inflammation by activated microglia/macrophages (Broekaart et al., 2018; Jurga et al., 2020). The resulting diffuse staining pattern (Figure 1h) made identification of individual cells and thus quantification of cell density difficult. Therefore, we determined the volume occupied by CD68 immunoreactivity in the hippocampal CA1 of sham- and KA-injected animals. Here, we observed a strong increase in immunoreactivity 5 days but not 4 h after KA injection, confirming that microglia/macrophages acquire a reactive phenotype after KA-induced SE (Figure 1l).

Taken together, these studies strongly suggest that hippocampal microglia become rapidly reactive following SE induction, even before the onset of neurodegeneration (Bedner et al., 2015). Ipsilaterally, the extent of innate immune cell activation gradually increased during the first two weeks of epileptogenesis. Transient microglial activation was also seen in the contralateral hippocampus.

3.2 | Microglia depletion prevents SE-induced GJ uncoupling

Loss of astrocytic GJ coupling is a characteristic feature of the sclerotic hippocampus in human and experimental TLE (Bedner et al., 2015). Our previous data suggest that the disruption of astrocyte coupling is mediated by microglia activation and release of pro-inflammatory cytokines (Bedner et al., 2015; Khan et al., 2016), although evidence for a causal relationship is still lacking. Thus, we employed the orally available CSF1R inhibitor PLX5622 (PLX) (Dagher et al., 2015) to deplete microglia from the brain prior to KA injection. Both non-injected and KA-injected (4 h post injection) FVB mice showed a 50%–60% reduction in IBA1-positive microglia in the hippocampus following 21 days of PLX treatment (non-injected: control diet 16,108 ± 1660 (mean ± SD) vs. PLX 21 d 6586 ± 982 cells/mm^3; KA-injected after 4 h: control diet 15,792 ± 2168 vs. PLX21d 7573 ± 952 cells/mm^3) (Figure 2a,b). Extending PLX administration to 28 days slightly increased depletion efficacy, but was nonetheless not sufficient to completely abolish microglia in the hippocampus (Figure S2a, b). Moreover, the reduction in IBA1-positive microglia was similar after 7 and 21 days of PLX treatment, indicating rapid clearance of microglia from the brain (Figure S2b). Tmem119 immunostaining

confirmed these findings, demonstrating high but incomplete microglia depletion (~70%) in KA mice subjected to 21 days of PLX treatment (Figure S2c,d). The extent of microglia depletion after PLX treatment was similar in C57B6J and FVB mice (Figure S2e,f). Finally, quantification of the morphology of surviving microglia after PLX treatment revealed no significant cytoskeletal changes compared to mice receiving a control diet (Figure S2g–k). To summarize, these findings contrast previous reports demonstrating almost complete removal of microglia from the brain after 3 weeks of continuous PLX treatment (Dagher et al., 2015). Nevertheless, our data show that CSF1R inhibition causes microglia depletion not only in the healthy but also the epileptic brain, making it a suitable approach to study the contribution of microglia to astrocyte dysfunction and epileptogenesis. Hence, in a next step we treated mice for 21 days with PLX prior to KA application and assessed GJ coupling 4 h later by biocytin filling of individual hippocampal CA1 *stratum radiatum* astrocytes. In the

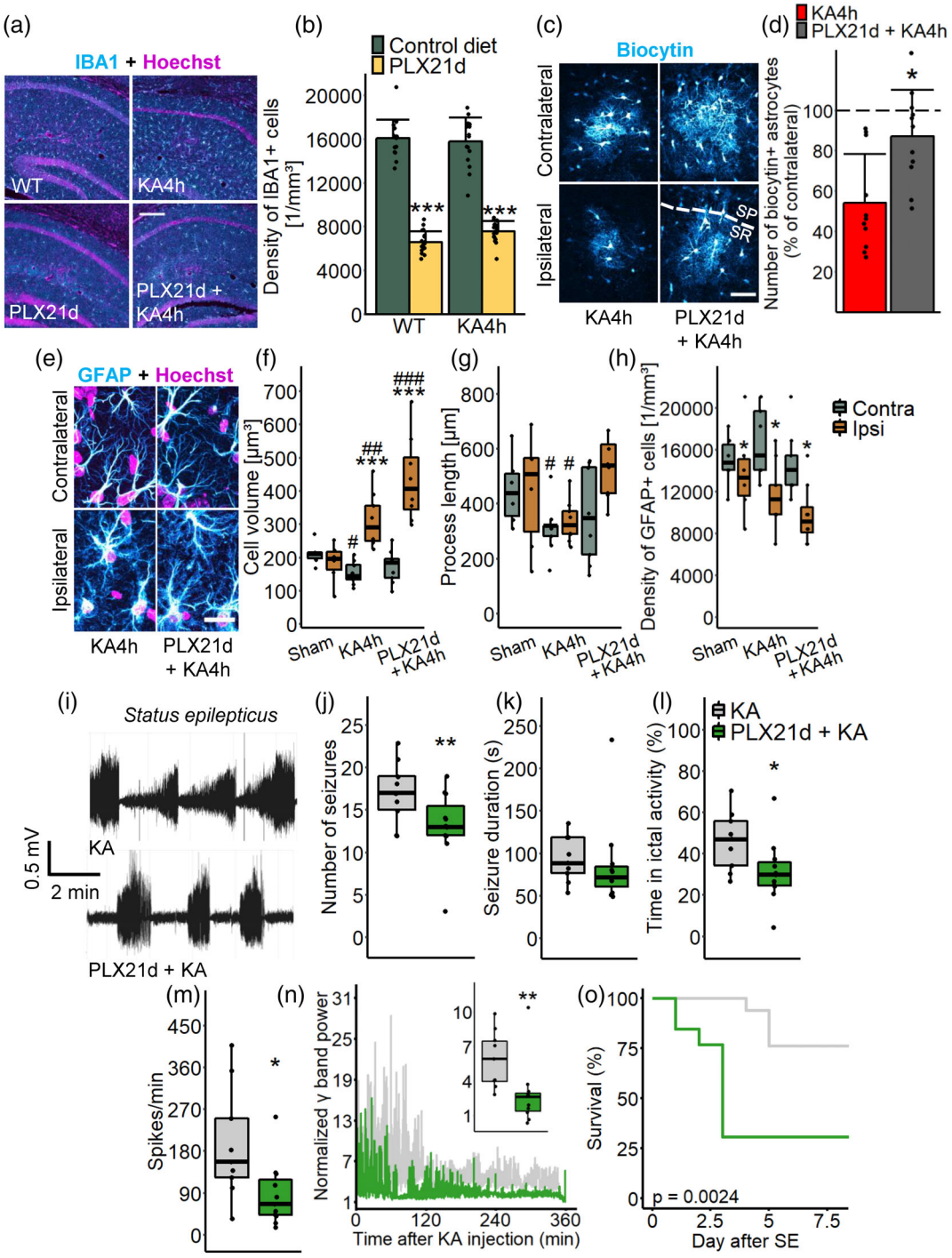

FIGURE 2 Legend on next page.

hippocampus of control mice, KA-induced SE led to a reduction of GJ coupling efficiency by about 50% at this time point (Bedner et al., 2015; Henning et al., 2021). Notably, PLX treatment and partial depletion of microglia completely prevented SE-induced uncoupling (KA 4 h: 54.14 ± 24.31% vs. PLX 21d + KA 4 h: 87.08 ± 23.03%; percentage of coupled astrocytes ipsi- vs. contralaterally) (Figure 2c,d).

Alterations in GFAP expression and morphology are considered hallmarks of reactive astrocytes (Escartin et al., 2021). Moreover, pro-inflammatory cytokines released from microglia have been shown to induce astrogliosis (Liddelow et al., 2017). To further elucidate the contribution of microglia to astrocyte reactivity during early KA-induced epileptogenesis, we characterized morphological features of GFAP-positive astrocytes in PLX-treated mice 4 h post KA injection in the CA1 *stratum radiatum*. Cell volume, total process length and cell density were quantified using 3D reconstructions derived from confocal images and compared between sham, KA and PLX21d + KA-treated mice (Figure 2e–h). The volume of GFAP-positive astrocytes was increased ipsilaterally and slightly decreased contralaterally, independent of whether mice were treated with PLX or not (Sham: ipsi 197, 164–218 vs. contra 212, 198–215 μm^3; KA 4 h: ipsi 291, 250–356 vs. contra 145, 135–178 μm^3; PLX 21 d + KA 4 h: ipsi 406, 345–501 vs. contra 184, 139–197 μm^3) (Figure 2f). The process lengths were reduced on both sides, an effect that could be prevented by PLX treatment (Sham: ipsi 508, 297–566 vs. contra 439, 356–508 μm; KA 4 h: ipsi 322, 290–373 vs. contra 320, 282–321 μm; PLX 21 d + KA 4 h: ipsi 538, 439–616 vs. contra 348, 216–532 μm) (Figure 2g). Consistent with our previously published data (Wu et al., 2021), the density of GFAP-positive cells was ipsilaterally decreased 4 h post KA, which was not prevented by PLX treatment (Figure 2h). A slight decrease in astrocyte density was also observed in the ipsilateral hippocampus of sham-injected mice (Sham: ipsi 13,352, 11,596–15,109 vs. contra 14,758, 14,055–16,515 cells/mm^3; KA 4 h: ipsi 11,244, 9839–12,650 vs. contra 15,461, 14,055–19,677 cells/mm^3; PLX 21 d + KA 4 h: ipsi 9136, 8082–10,541 vs. contra 14,055, 12,650–15,461 cells/mm^3) (Figure 2h). In conclusion, our data reveal that in addition to microglia, astrocytes become rapidly reactive following SE induction. However, partial microglia depletion only slightly affected the morphological alterations these cells underwent 4 h after onset of SE.

3.3 | Microglia depletion attenuates the severity of KA-induced SE but increases mortality

The protective effect of PLX treatment on astrocyte coupling prompted us to examine the consequences of microglia depletion on epileptogenesis in our TLE-HS model. As astrocyte uncoupling is thought to causally contribute to epileptogenesis (Bedner et al., 2015; Deshpande et al., 2020; Onodera et al., 2021), we hypothesized that PLX exerts antiepileptogenic effects in our model. A subset of mice was treated with PLX for 21 days and subsequently subjected to intracortical KA injection, which was immediately followed by implantation of telemetric EEG transmitters. A control group received standard chow prior to KA injection and transmitter implantation. We quantified the severity of SE, which in our model is manifested by a series of convulsive seizures (Figure 2i) lasting up to several hours. The number of seizures, their duration and the overall time spent in ictal activity was quantified during the first h of SE. Additionally, we counted the number of epileptic spikes during the first 6 h of recording and compared the spectral power in the γ range after fast Fourier transformation (FFT) of the EEG data. Baseline activity did not differ between groups ($p = 0.99$, independent samples *t*-test; data not shown). We detected significantly less seizures (KA: 17, 15–19 vs. PLX 21 d + KA: 13, 12–16 seizures) and a reduced time spent in ictal activity (KA: 47, 34–56 vs. PLX 21 d + KA: 30, 25%–36%) in PLX-treated compared to control mice during the first hour of KA-induced SE (Figure 2j,l) whereas seizure duration was not affected (KA: 89, 77–119 vs. PLX 21 d + KA: 71, 61–84 s) (Figure 2k). To further

FIGURE 2 Microglia depletion prevents astrocytic uncoupling and attenuates SE severity. (a) Representative MIPs of a combined IBA1 and Hoechst staining in the hippocampus of non-injected mice fed a control diet (non-injected), PLX-treated (PLX 21 days), KA-injected (KA 4 h) and PLX- + KA-treated (PLX 21 days + KA 4 h) FVB mice. Scale bar: 200 μm. (b) The number of IBA1-positive cells was reduced by 50%–60% in the hippocampus of both, KA- and non-injected mice receiving PLX-diet (1200 mg/kg). $n = 3$ slices/mouse, $N = 3$ mice/condition; one-way ANOVA; * versus control diet. (c) Representative MIPs depicting biocytin-filled astrocytes labeled with streptavidin-conjugated Alexa Fluor® 647 in the ipsi- and contralateral hippocampal CA1 *stratum radiatum* region in KA-injected (KA 4 h) and PLX- + KA-treated (PLX 21 days + KA 4 h) FVB mice 4 h post KA injection. Images depict a background subtracted and brightness adjusted ROI representative of the whole coupling cloud. Scale bar: 50 μm. (d) Partial microglia depletion prevented GJ uncoupling of astrocytes during SE. $n = 11$ cells/condition, $N = 4$ mice; Independent samples *t*-test. The dashed line indicates the value of the contralateral hemisphere; * versus KA4h. (e) Representative MIPs of combined GFAP and Hoechst staining in the ipsi- and contralateral hippocampal CA1 *stratum radiatum* of mice with or without PLX pre-treatment, 4 h after KA injection. Scale bar: 20 μm. (f–h) Analyses of volume, total process length and density of GFAP-positive astrocytes revealed that microglia depletion only marginally affects astrogliosis. $n = 3$ slices/mouse, $N = 3$ mice/condition; two-way ANOVA; * versus contra, # versus sham. (I) Representative EEG traces during KA-induced SE in PLX-untreated (top) and PLX-treated (bottom) mice. (j–l) Number of seizures, seizure duration, and time spent in ictal activity during the first h of SE. PLX pre-treatment reduced number and time spent in seizures but not seizure duration. $N = 9$ KA and 11 PLX21d + KA mice; independent samples *t*-test; * versus KA. (m, n) The number of spikes per min as well as high frequency EEG activity ($\gamma = 30–50$ Hz) were reduced in PLX-treated mice during the first 6 h after KA injection. $N = 9$ KA and 11 PLX21d + KA mice; Wilcoxon rank sum test; * versus KA. (o) Kaplan–Meier curve showing that the mortality was increased in PLX-treated compared to untreated mice following KA injection. $N = 17$ KA and 13 PLX21d + KA mice; log-rank test. Data are displayed as box plots representing median and quartiles, or as bar graphs with mean + SD. Black dots represent individual data points. SR, *stratum radiatum*; SP, *stratum pyramidale*. $^*p < 0.05$; $^{**}p < 0.05$; $^{***}p < 0.001$; $\#p < 0.05$; $\#\#p < 0.01$; $\#\#\#p < 0.001$

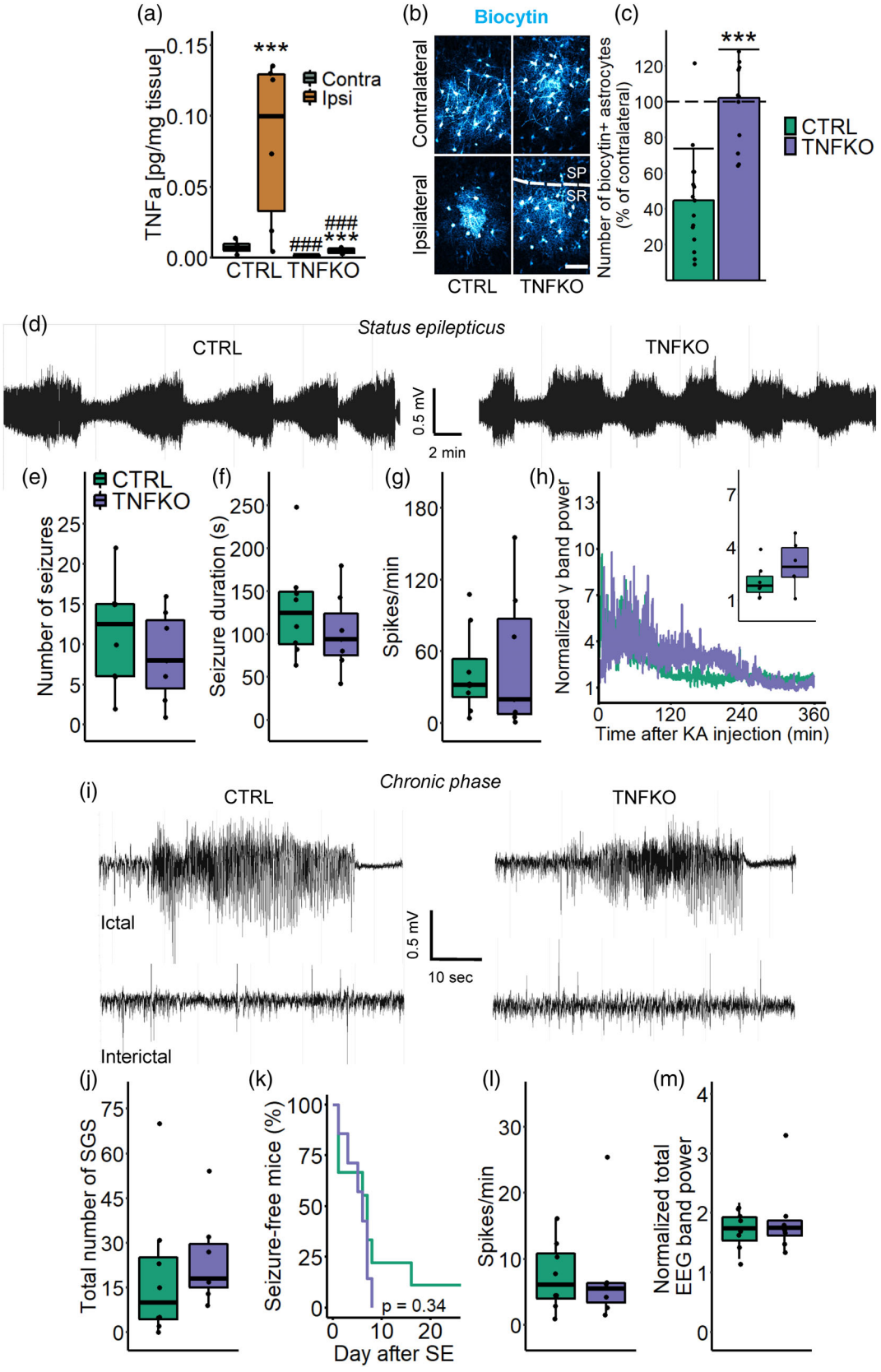

FIGURE 3 Legend on next page.

characterize SE, spike and spectral analyses were performed during an extended period of 6 h after SE induction. Both spike number (KA: 158, 124–251 vs. PLX 21 d + KA: 66, 43–119 spikes/min) and high-frequency activity in the γ range (KA: 5, 3.97–7.13 vs. PLX 21 d + KA: 2.6, 1.38–2.93) were significantly reduced in PLX-treated versus control mice (Figure 2m,n). Unexpectedly, PLX treatment significantly increased the mortality rate of KA injected mice (KA: 21.43% (3 of 14 mice) vs. PLX 21 d + KA: 69.23% (9 of 13 mice)) (Figure 2o), which made long-term investigations of the chronic phase impossible. Together, the data show that partial microglia depletion reduces the severity of KA-induced SE, implicating microglia as modulators of epileptiform activity.

3.4 | SE-induced uncoupling of astrocytes requires TNFα released from microglia

So far, our data (Figure 2) support a role for activated microglia in astrocyte uncoupling and ictogenesis following KA-induced SE, and we hypothesized that microglia exert their detrimental effects *via* the release of TNFα. To explore this hypothesis, we subjected microglia-specific and inducible TNFα knockout (TNFKO) mice to our TLE model and performed ELISA to quantify hippocampal TNFα concentrations 4 h post KA injection. TNFα levels were strongly increased in the ipsilateral hippocampus of heterozygous Cre-expressing control (CTRL) mice (ipsi 0.126, 0.074–0.13; contra 0.006, 0.005–0.009 pg/mg tissue) (Figure 3a). Although in TNFKO versus CTRL mice the ipsilateral TNFα level upon KA injection was markedly reduced, it was still higher than on the contralateral side (TNFKO: ipsi 0.005, 0.003–0.006; contra 0.001, 0.001–0.001 pg/mg tissue) (Figure 3a). Nevertheless, this ipsilateral reduction of TNFα in TNFKO mice was sufficient to completely prevent the 50% loss of astrocyte GJ coupling occurring in CTRL mice 4 h post KA injection (CTRL: 44.75 ± 28.91% vs. TNFKO: 102 ± 27.07%; percentage of coupled astrocytes ipsi- vs. contralaterally) (Figure 3b,c). Although single-cell transcript analysis did not detect significant changes in TNFR1 and TNFR2 mRNA expression levels (Figure S3a,b), there was a significant increase in TNFR1 immunoreactivity in GFAP-positive astrocytes at both 4 h and 5 days post KA injection (Figure S3g,h). Collectively, these data provide evidence that during early epileptogenesis, microglia are a primary source of pro-inflammatory TNFα, which impairs astrocytic GJ coupling, probably via TNFR1 signaling.

3.5 | Microglia-specific reduction of TNFα does not affect KA-induced SE and subsequent generation of spontaneous seizure activity

Next, we used continuous EEG monitoring to address the question whether KA-induced SE and spontaneous seizure generation are affected in TNFKO mice over the first 4 weeks after KA injection. During the first hour of SE, neither the number of seizures (CTRL 12.5, 6–15 vs. TNFKO 8, 4.5–13 seizures) nor seizure duration (CTRL 125, 88–149 vs. TNFKO 94, 75–149 s) differed between genotypes (Figure 3e,f). During the first 6 h after KA injection the number of spikes (CTRL 11506, 7784–19,223 vs. TNFKO 7018, 2682–31,412 spikes/min) and high frequency EEG activity (CTRL 1.81, 1.44–2.35 vs. TNFKO 2.88, 2.3–3.97) were also similar (Figure 3g,h). Mortality was not different between both genotypes (data not shown). During the chronic phase (4 weeks post KA injection), the total number of spontaneous generalized seizures (SGS) did not differ between the genotypes (CTRL 10, 4.25–25 vs. TNFKO 18, 15–29.5 SGS) (Figure 3j). Likewise, the length of the latent phase was not influenced by the lack of microglial TNFα (CTRL 8.33 ± 8.77 vs. TNFKO 5.29 ± 2.5 days until first SGS) (Figure 3k). Finally, neither the total number of epileptic spikes per min (CTRL 6.25, 3.91–10.57 vs. TNFKO 3.78, 2.41–5.29 spikes/min) nor the total EEG band power (CTRL 1.75, 1.54–1.93 vs. TNFKO 1.75, 1.62–1.87) were different between experimental groups (Figure 3l,m). Taken together, these results indicate that the microglia-specific reduction of TNFα levels in TNFKO mice was insufficient to attenuate KA-induced SE or chronic seizure activity in our TLE model.

FIGURE 3 Reducing microglial TNFα prevented astrocytic uncoupling but did not attenuate seizure activity during SE and the chronic phase. (a) Tissue concentration of TNFα determined by ELISA was significantly increased 4 h after KA injection in the ipsi- versus contralateral dorsal hippocampus of both, Cx3cr1$^{CreERT2/+}$-TNFα$^{+/+}$ (CTRL) and Cx3cr1$^{CreERT2/+}$-TNFα$^{loxp/loxp}$ (TNFKO) mice, but the increase in TNFKO mice was significantly lower ($N = 5$ CTRL and 8 TNFKO mice; two-way ANOVA; * vs. ipsi, # vs. CTRL). (b) Representative MIPs depicting biocytin-positive astrocytes 4 h post KA injection in the ipsi- and contralateral hippocampal CA1 *stratum radiatum* of CTRL and TNFKO mice. Scale bar: 50 μm. Images depict a background subtracted and brightness adjusted ROI representative of the whole coupling cloud. (c) Microglia-specific knockout of TNFα prevents uncoupling of astrocytes 4 h post KA injection. $n = 12–15$ cells/condition, $N = 4–5$ mice; Independent samples *t*-test. The dashed line indicates the value on the contralateral hemisphere; * versus CTRL. (d) Representative EEG traces during SE in TNFKO and CTRL mice. (e, f) No differences between groups regarding number and duration of seizures during the first h of SE were found. (g, h) Similarly, analyses of spike frequency and normalized γ band EEG activity during the first 6 h of EEG recording revealed no difference between genotypes (inset displays the median γ band activity over 6 h of SE). (i) Representative EEG traces (ictal activity, top; interictal, bottom) from TNFKO and CTRL mice during week 4 after KA injection. (j, k) Total number of SGS and the length of the latent phase did not differ between genotypes. (l, m) Spike frequency and normalized total EEG band power were similar in both groups. $N = 7$ TNFKO and 8 CTRL mice. Data are displayed as box plots representing median and quartiles and were analysed using either an independent samples *t*-test, a Wilcoxon rank sum test or a log-rank test. Black dots represent individual data points. SR, *stratum radiatum*; SP, *stratum pyramidale*. ***$p < 0.001$; ###$p < 0.001$

3.6 | Reduced TNFα release from microglia did not affect neurodegeneration but attenuated astro- and microgliosis in KA-induced TLE

Approximately two-thirds of patients with pharmacoresistant TLE exhibit HS, which is characterized by marked neurodegeneration, reactive astro- and microgliosis, and GCD (Aronica et al., 2007; Blümcke et al., 1999; Broekaart et al., 2018). These histopathological changes are well reproduced in our mouse model of TLE (Bedner et al., 2015; Deshpande et al., 2020). To determine whether reduction of microglial TNFα influences HS development, we immunostained hippocampal slices with antibodies against NeuN, GFAP, and Hoechst 4 weeks after epilepsy induction (Figure 4a). Hippocampal neurodegeneration, GCD and shrinkage of the CA1 *stratum radiatum* were similar in the hippocampus of KA-injected CTRL and TNFKO mice (number of CA1 neurons: CTRL: ipsi 19, 9.5–24 vs. contra 71.5, 60–82.5; TNFKO: ipsi 25, 4–63 vs. contra 62, 53.5–74; *stratum radiatum* width: CTRL: ipsi 134.38, 84.81–147.92 vs. contra 185.4, 159.6–198.6 μm; TNFKO: ipsi 112.50, 72.15–152.65 vs. contra 179.8, 167.8–194.5 μm; GCD: CTRL: ipsi 78, 68.34–91-13 vs. contra 84.74, 71.33–99.85 μm; TNFKO: ipsi 86.83, 83.17–121.63 vs. contra 82.43, 70.86–89.03 μm) (Figure 4b–d). Next, the degree of astrogliosis in the hippocampal CA1 *stratum radiatum* based on the total volume occupied by the GFAP signal was quantified using a custom-written algorithm in FIJI. GFAP immunoreactivity was increased ipsi- vs. contralaterally in both genotypes, but this increase was less pronounced in TNFKO mice (CTRL (mean ± SD): ipsi 4.5 ± 1.35 vs. contra 3 ± 1.21%; TNFKO: ipsi 3.87 ± 1.65 vs. contra 2.33 ± 0.91%) (Figure 4e). Finally, we determined the magnitude of microglia/macrophage activation by quantifying the volume occupied by IBA1-positive

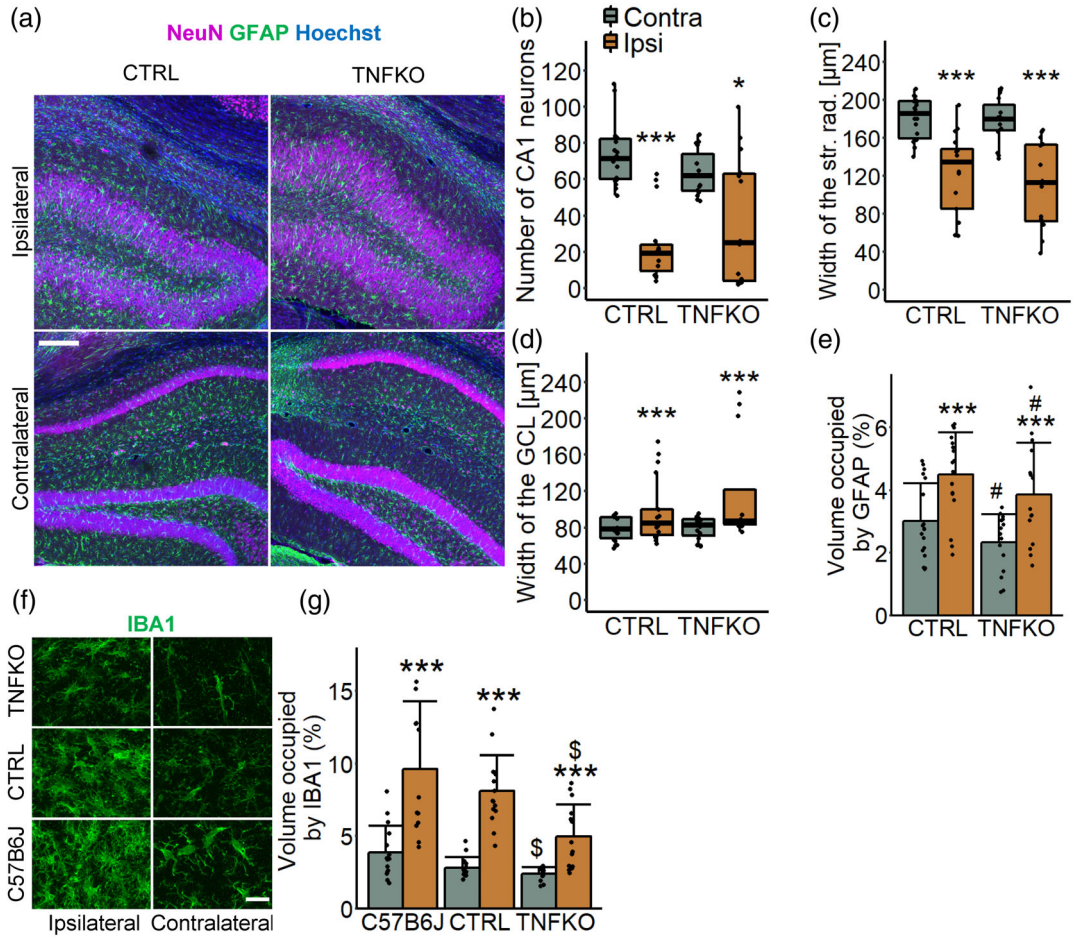

FIGURE 4 Microglia-specific reduction of TNFα attenuates astro- and microgliosis 4 weeks after KA-injection. (a) Representative MIPs of combined NeuN (magenta), GFAP (green), and Hoechst (blue) staining in ipsi- and contralateral hippocampal slices from CTRL and TNFKO mice obtained 4 weeks after KA injection. Scale bar: 200 μm. (b–e) KA-injected CTRL and TNFKO mice displayed similar pyramidal cell loss in the CA1 region, shrinkage of the *stratum radiatum* and GCD, while astrogliosis in the CA1 *stratum radiatum* was less pronounced both ipsi- and contralaterally in TNFKO mice. $n = 3$ slices/mouse, $N = 6$ CTRL and 5 TNFKO mice; * versus contra, # versus CTRL. (f) Representative MIPs of IBA1 staining in the ipsi- and contralateral hippocampal CA1 *stratum radiatum* from C57B6J, CTRL and TNFKO mice 4 weeks after KA injection. Scale bar: 20 μm. (g) Microgliosis was present in all genotypes in the ipsilateral hippocampus, but overall reduced in KA-treated TNFKO compared to C57B6J mice. $n = 2–3$ slices/mouse, $N = 5$ mice/condition; * versus ipsi; $ versus C57B6J. Data are displayed as box plots representing median and quartiles or as bar graphs with mean + SD and were analysed using two-way ANOVA. Black dots represent individual data points. CA, cornu ammonis; str. rad., *stratum radiatum*; GCL, granule cell layer. ***$p < 0.001$; *$p < 0.05$; #$p < 0.05$; $$p < 0.05$

cells in the hippocampus of C57B6J, CTRL and TNFKO mice, 4 weeks post KA-induced SE (Figure 4f,g). The data revealed a pronounced increase in IBA1 immunoreactivity in ipsilateral hippocampi across all genotypes. While no differences were found in CTRL versus C57B6J and CTRL versus TNFKO mice, IBA1 immunoreactivity was significantly attenuated both ipsi- and contralaterally, in TNFKO compared to C57B6J mice (C57B6J: ipsi 9.60 ± 4.66 vs. contra 3.87 ± 1.83%; CTRL: ipsi 8.11 ± 2.45 vs. contra 2.82 ± 0.71%; TNFKO: ipsi 4.95 ± 2.24 vs. contra 2.41 ± 0.45%) (Figure 4f,g). Thus, during the first 4 weeks of epileptogenesis, microglia-derived TNFα specifically promotes astrogliosis and innate immune cell activation while neurodegeneration and GCD are less sensitive.

4 | DISCUSSION

In the present study we show that microglia become rapidly and chronically activated in a mouse model closely resembling key features of human TLE (Bedner et al., 2015). By combining pharmacology and cell-type-specific gene knockout we identified microglia as major drivers of early TNFα production, severity of SE, reactive gliosis, and uncoupling of hippocampal astrocytes following KA injection. Microglia activation temporally preceded neuronal cell death and was also transiently detectable in the contralateral hippocampus, indicating that it was not a response to neurodegeneration, but rather a result of seizure activity *per se* (Bedner et al., 2015). Indeed, microglia register neuronal hyperactivity during KA-induced SE *via* a mechanism involving glutamate-dependent ATP release from neurons, which is sensed by microglial P2Y12 receptors (Dissing-Olesen et al., 2014; Eyo et al., 2014). Our stereological analyses revealed a dramatic increase in the number of IBA1-positive cells during the latent and chronic phases of epilepsy. Moreover, the extent of innate immune cell activation gradually increased over time, which was indicated by the appearance of CD68, a marker of activated macrophages (Jurga et al., 2020). Both microglia and infiltrated monocytes jointly contribute to the pool of activated innate immune cells in experimental TLE (Feng et al., 2019; Käufer et al., 2018; Waltl, Käufer, Bröer, et al., 2018), and invasion of blood-borne monocytes exacerbates neurodegeneration, blood–brain barrier (BBB) breakdown and inflammation following SE (Varvel et al., 2016). Our data revealed the emergence of CD169-positive cells at later time points (i.e., 5 and 14 days post KA injection), indicating monocyte infiltration after KA injection. However, co-staining of CD169 with the microglia-specific marker Tmem119 at 5 days post KA injection questioned the specificity of CD169 as a marker of infiltrating monocytes. In support of this, reactive microglia have been shown to upregulate CD169 in other pathological conditions, such as following lipopolysaccharide (LPS) exposure and in experimental autoimmune encephalomyelitis (Bennett et al., 2016; Bogie et al., 2018). Nevertheless, it is possible that the CD169-positive/Tmem119-negative cells detected in the ipsilateral hippocampus are monocytes that have crossed the compromised BBB characteristic of our TLE model (Deshpande et al., 2017; Henning et al., 2021). Notably, the density of IBA1 and CD169 immunoreactive cells was also transiently increased in the contralateral hippocampus. Whether contralateral innate immune cell activation contributes to the pathology of epilepsy remains to be established.

To study microglial contributions to epileptogenesis, we examined consequences of microglia depletion by applying the CSF1R inhibitor PLX5622 prior to KA injection. In contrast to previous observations (Basilico et al., 2022; Dagher et al., 2015), in the present study PLX only partially depleted microglia, regardless of the duration of application, mouse genotype or microglial markers employed. The morphology of PLX-resistant microglia remained unchanged. The reasons for the incomplete depletion remain unclear, as our mice had *ad libitum* access to the PLX-supplemented diet and readily consumed it (3–4 g/mouse/day). Nevertheless, this incomplete depletion was sufficient to completely prevent loss of astrocyte GJ coupling and to mitigate the severity of KA-induced SE. Together, these findings are consistent with our hypothesis that microglia indirectly promote epileptogenesis by decreasing GJ-mediated K^+ and glutamate buffering capacity of astrocytes, and are in line with previous studies that have identified microglia as drivers of neuronal hyperactivity and seizures (Pascual et al., 2012; Riazi et al., 2008; Rodgers et al., 2009). It should be noted, however, that other studies did not find evidence for a role of microglia in modulating KA- or pilocarpine- induced seizures (Altmann et al., 2022; Feng et al., 2019; Mirrione et al., 2010) or even reported increased SE severity after microglia depletion (Liu et al., 2020; Wu et al., 2020). Possible explanations underlying these discrepancies include differences between animal models and efficiency of microglia depletion.

Our stereological data revealed that astrocyte morphology changes are rapidly induced and occur in parallel with microglia activation upon SE induction. In addition, partial microglia depletion had only minor effects on astrocyte morphology changes during SE. This is in contrast to a previous study, showing that microglia activation precedes astrocyte reactivity and that depletion of microglia is sufficient to prevent morphological alterations of astrocytes after pilocarpine-induced SE (Sano et al., 2021). The lack of effect in the present study could be due to the incomplete depletion of microglia in our model. Alternatively, as astrocytes sense neuronal activity via a variety of ion channels and neurotransmitter receptors (Coulter & Steinhauser, 2015), astrocyte morphology changes in response to hyperactivity may be largely independent of inflammatory signaling by microglia.

To our surprise, microglia-depleted mice exhibited high mortality following KA-injection, a phenomenon that was also observed in other studies of SE- and infection-induced epilepsy (Sanchez et al., 2019; Waltl, Käufer, Gerhauser, et al., 2018; Wu et al., 2020). These studies showed that microglia depletion exacerbates neurodegeneration following an epileptogenic insult, indicating that microglia serve neuroprotective functions in epilepsy (Sanchez et al., 2019; Waltl et al., 2018; Wu et al., 2020). However, CSF1R is expressed in all myeloid cells of the body and CSF1R inhibition has been shown to reduce peripheral macrophage numbers (Green et al., 2020; Merry et al., 2020). Since macrophages play an important role in wound healing (Kim & Nair, 2019), reduced macrophage numbers following PLX treatment could have increased mortality due to impaired

regeneration after surgical EEG implantation. Thus, whether the increased mortality after microglia depletion in our model reflects a protective role of microglia in epilepsy or merely the peripheral side effects of blocking CSF1R, remains to be clarified. The observed increase in mortality after PLX treatment in our model nevertheless implies that microglia depletion does not represent a compelling strategy for the treatment of epilepsy and emphasizes the need for more targeted microglial manipulations in TLE.

The opposing effects of microglia depletion in our model prompted us to manipulate these cells in such a way that the antiepileptic aspects of PLX treatment are retained while simultaneously preserving essential functions of microglia for survival of the animals. We hypothesized that preventing the release of the pro-inflammatory cytokine TNFα from microglia could be a promising strategy, as the cytokine has previously been associated with both astrocyte reactivity and epilepsy (Liddelow et al., 2017; Patel et al., 2017). Using microglia-specific inducible TNFα knockout mice, we identified microglia as the primary source of TNFα 4 h after KA injection. This finding is in line with studies demonstrating that microglia are major producers of TNFα following pilocarpine-induced SE (Sano et al., 2021; Wang et al., 2015). Importantly, reduction of TNFα in microglia prevented early astrocyte uncoupling, confirming that the loss of coupling in wild type mice after KA-induced SE (Bedner et al., 2015) depends on TNFα signaling. Our immunohistochemical analyses further revealed increased TNFR1 expression in astrocytes at 4 h and 5 days post KA injection, suggesting that microglial TNFα acts via TNFR1 to impair GJ coupling in astrocytes.

In contrast to our expectations, microglia-specific TNFα knockout had no effects on SE or chronic epileptiform activity in our model. There are several possible explanations for this finding. First, it cannot be excluded that residual release of the cytokine still occurs in tamoxifen-treated TNFKO mice upon KA-induced SE and contributes to the ipsilateral increase we have observed, which might be sufficient to generate hyperactivity. Moreover, experimental data from various pathological conditions show that TNFα has antithetical effects depending on whether it signals via TNFR1 or TNFR2 (Balosso et al., 2005; Brambilla et al., 2011; Dong et al., 2016; Karamita et al., 2017; Patel et al., 2017; Weinberg et al., 2013). In the context of epilepsy, Balosso et al. (2005) demonstrated that the susceptibility to KA-induced acute seizures was reduced in mice lacking TNFR1 but increased in mice lacking TNFR2. Similarly, in a study by Patel et al. (2017) it was shown that combined knockout of TNFR1/TNFR2 decreased acute infection-induced seizures, while selective TNFR2 deletion led to exacerbation of seizures. Thus, it is possible that reduction of TNFα in microglia has no consequence on seizure activity in our model because deleterious and beneficial effects of TNFα signaling via TNFR1 and TNFR2 cancel out each other. While our data show that microglia are the primary source of TNFα released during SE, other immunocompetent cells might contribute to TNFα release at later stages of epileptogenesis, e.g. peripheral monocytes upon infiltration into the CNS. In the present study, TNFα reduction was restricted to microglia by maintaining a sufficiently long interval between tamoxifen and KA injection, thus exploiting the much faster turnover rates of peripheral monocytes compared to microglia (Goldmann et al., 2013; Parkhurst et al., 2013). Conversely, shortening the interval between tamoxifen and KA injections would allow to investigate whether combined reduction of TNFα in microglia and peripheral monocytes attenuates seizure activity in our TLE model. The discrepancy between the data from our PLX and TNFKO experiments in terms of affecting SE severity might indicate that factors other than microglia-derived TNFα contribute to the susceptibility to KA-induced seizures. Indeed, microglia release several pro-inflammatory cytokines that modulate seizures, including interleukin (IL)-1ß (Vezzani et al., 1999, 2011). Additionally, a non-inflammatory reactive microglial state caused by genetic overactivation of mTOR and characterized by increased phagocytic activity has been shown to be sufficient to cause epileptic activity (Zhao et al., 2018). Thus, partial microglia depletion using PLX may have prevented phenotypic changes of microglia other than TNFα release, which might explain its seizure suppressing effects during KA-induced SE. The identification of microglia-derived factors underlying the beneficial effect of PLX on KA-induced seizures as seen in the present study requires further investigations.

In the present study microglia-specific TNFα knockout attenuated astrogliosis and immune cell activation, but did not attenuate neurodegeneration, GCD and *stratum radiatum* shrinkage during the chronic phase of epilepsy. Limited recombination efficiency or simultaneous modulation of TNFR1 and TNFR2 signaling may be responsible for the latter, as discussed above. For example, inhibition of TNFR1 was shown to ameliorate hippocampal cell death in KA-induced epilepsy (Weinberg et al., 2013), whereas increased neuronal loss occurred in mice lacking both TNFRs (Bruce et al., 1996). Thus, specifically targeting the TNFα-TNFR1 axis might represent a promising strategy to attenuate SE-induced neurodegeneration.

5 | CONCLUSION

The present study provides novel insights into the role of microglia reactivity and TNFα release in astrocyte dysfunction and epileptogenesis. During KA-induced SE, microglia become rapidly reactive and constitute a primary source of TNFα, which targets astrocytes, impairs GJ coupling and contributes to the development of TLE. The observations of the present study reveal additional mechanisms underlying inflammation-induced epileptogenesis and emphasize the importance of targeted anti-inflammatory treatments in TLE.

ACKNOWLEDGMENTS

The authors thank Francesco Santarelli for help with performing the TNFα ELISA. PLX5622 was provided under Materials Transfer Agreement by Plexxikon Inc. (Berkeley, CA). Open Access funding enabled and organized by Projekt DEAL.

FUNDING INFORMATION

This research was supported by the EU (H2020-MSCA-ITN project 722053 EU-GliaPhD; to CS) and BMBF (16GW0182 CONNEXIN, 01DN20001 CONNEX; to CS).

CONFLICT OF INTEREST

The authors declare that they have no conflict of interest.

DATA AVAILABILITY STATEMENT

The data that support the findings of this study are available from the corresponding author upon reasonable request.

ORCID

Christian Steinhäuser https://orcid.org/0000-0003-2579-8357
Peter Bedner https://orcid.org/0000-0003-0090-7553

REFERENCES

Altmann, A., Ryten, M., Di Nunzio, M., Ravizza, T., Tolomeo, D., Reynolds, R. H., Somani, A., Bacigaluppi, M., Iori, V., Micotti, E., Di Sapia, R., Cerovic, M., Palma, E., Ruffolo, G., Botía, J. A., Absil, J., Alhusaini, S., Alvim, M., Auvinen, P., … Sisodiya, S. M. (2022). A systems-level analysis highlights microglial activation as a modifying factor in common epilepsies. *Neuropathology and Applied Neurobiology*, *48* (1), e12758. https://doi.org/10.1111/nan.12758

Aronica, E., Boer, K., van Vliet, E. A., Redeker, S., Baayen, J. C., Spliet, W. G. M.van Rijen, P. C., Troost, D., Lopes da Silva, F. H., Wadman, W. J., & Gorter, J. A. (2007). Complement activation in experimental and human temporal lobe epilepsy. *Neurobiology of Disease*, *26* (3), 497–511. https://doi.org/10.1016/j.nbd.2007.01.015

Aronica, E., Bauer, S., Bozzi, Y., Caleo, M., Dingledine, R., Gorter, J. A., Henshall, D. C., Kaufer, D., Koh, S., Löscher, W., Louboutin, J.-P., Mishto, M., Norwood, B. A., Palma, E., Poulter, M. O., Terrone, G., Vezzani, A., & Kaminski, R. M. (2017). Neuroinflammatory targets and treatments for epilepsy validated in experimental models. *Epilepsia*, *58*, 27–38. https://doi.org/10.1111/epi.13783

Avignone, E., Ulmann, L., Levavasseur, F., Rassendren, F., & Audinat, E. (2008). Status epilepticus induces a particular microglial activation state characterized by enhanced purinergic signaling. *Journal of Neuroscience*, *28*(37), 9133–9144. https://doi.org/10.1523/JNEUROSCI.1820-08.2008

Balosso, S., Ravizza, T., Perego, C., Peschon, J., Campbell, I. L., De Simoni, M. G., & Vezzani, A. (2005). Tumor necrosis factor-α inhibits seizures in mice via p75 receptors. *Annals of Neurology*, *57*(6), 804–812. https://doi.org/10.1002/ana.20480

Basilico, B., Ferrucci, L., Ratano, P., Golia, M. T., Grimaldi, A., Rosito, M., Ferretti, V., Reverte, I., Sanchini, C., Marrone, M. C., Giubettini, M., De Turris, V., Salerno, D., Garofalo, S., St-Pierre, M. K., Carrier, M., Renzi, M., Pagani, F., Modi, B., … Ragozzino, D. (2022). Microglia control glutamatergic synapses in the adult mouse hippocampus. *Glia*, *70*(1), 173–195. https://doi.org/10.1002/glia.24101

Bedner, P., Dupper, A., Hüttmann, K., Müller, J., Herde, M. K., Dublin, P., Deshpande, T., Schramm, J., Häussler, C. A., Henneberger, C., Theis, M., & Steinhäuser, C. (2015). Astrocyte uncoupling as a cause of human temporal lobe epilepsy. *Brain*, *138*(5), 1208–1222. https://doi.org/10.1093/brain/awv067

Bennett, M. L., Bennett, F. C., Liddelow, S. A., Ajami, B., Zamanian, J. L., Fernhoff, N. B., Mulinyawe, S. B., Bohlen, C. J., Adil, A., Tucker, A., Weissman, I. L., Chang, E. F., Li, G., Grant, G. A., Hayden Gephart, M. G., & Barres, B. A. (2016). New tools for studying microglia in the mouse and human CNS. *Proceedings of the National Academy of Sciences*, *113* (12), E1738–E1746. https://doi.org/10.1073/pnas.1525528113

Benson, M. J., Manzanero, S., & Borges, K. (2015). Complex alterations in microglial M1/M2 markers during the development of epilepsy in two mouse models. *Epilepsia*, *56*(6), 895–905. https://doi.org/10.1111/epi.12960

Blümcke, I., Beck, H., Lie, A. A., & Wiestler, O. D. (1999). Molecular neuropathology of human mesial temporal lobe epilepsy. *Epilepsy Research*, *36*(2–3), 205–223. https://doi.org/10.1016/S0920-1211(99)00052-2

Bogie, J. F., Boelen, E., Louagie, E., Delputte, P., Elewaut, D., van Horssen, J. Hendriks, J. J., & Hellings, N. (2018). CD169 is a marker for highly pathogenic phagocytes in multiple sclerosis. *Multiple Sclerosis Journal*, *24*(3), 290–300. https://doi.org/10.1177/1352458517698759

Brambilla, R., Ashbaugh, J. J., Magliozzi, R., Dellarole, A., Karmally, S., Szymkowski, D. E., & Bethea, J. R. (2011). Inhibition of soluble tumour necrosis factor is therapeutic in experimental autoimmune encephalomyelitis and promotes axon preservation and remyelination. *Brain*, *134* (9), 2736–2754. https://doi.org/10.1093/brain/awr199

Broekaart, D. W. M., Anink, J. J., Baayen, J. C., Idema, S., de Vries, H. E., Aronica, E., Gorter, J. J., & van Vliet, E. A. (2018). Activation of the innate immune system is evident throughout epileptogenesis and is associated with blood-brain barrier dysfunction and seizure progression. *Epilepsia*, *59*(10), 1931–1944. https://doi.org/10.1111/epi.14550

Bruce, A. J., Boling, W., Kindy, M. S., Peschon, J., Kraemer, P. J., Carpenter, M. K., Holtsberg, F. W., & Mattson, M. P. (1996). Altered neuronal and microglial responses to excitotoxic and ischemic brain injury in mice lacking TNF receptors. *Nature Medicine*, *2*(7), 788–794. https://doi.org/10.1038/nm0796-788

Butovsky, O., Siddiqui, S., Gabriely, G., Lanser, A. J., Dake, B., Murugaiyan, G., Doykan, C. E., Wu, P. M., Gali, R. R., Iyer, L. K., Lawson, R., Berry, J., Krichevsky, A. M., Cudkowicz, M. E., & Weiner, H. L. (2012). Modulating inflammatory monocytes with a unique microRNA gene signature ameliorates murine ALS. *Journal of Clinical Investigation*, *122*(9), 3063–3087. https://doi.org/10.1172/JCI62636

Coulter, D. A., & Steinhauser, C. (2015). Role of Astrocytes in Epilepsy. *Cold Spring Harbor Perspectives in Medicine*, *5*(3), a022434. https://doi.org/10.1101/cshperspect.a022434

Dagher, N. N., Najafi, A. R., Kayala, K. M. N., Elmore, M. R. P., White, T. E., Medeiros, R., West, B. L., & Green, K. N. (2015). Colony-stimulating factor 1 receptor inhibition prevents microglial plaque association and improves cognition in 3xTg-AD mice. *Journal of Neuroinflammation*, *12* (1), 139. https://doi.org/10.1186/s12974-015-0366-9

De Simoni, M. G., Perego, C., Ravizza, T., Moneta, D., Conti, M., Marchesi, F., Garattini, S., & Vezzani, A. (2000). Inflammatory cytokines and related genes are induced in the rat hippocampus by limbic status epilepticus: Cytokines in status epilepticus. *European Journal of Neuroscience*, *12*(7), 2623–2633. https://doi.org/10.1046/j.1460-9568.2000.00140.x

Deshpande, T., Li, T., Henning, L., Wu, Z., Müller, J., Seifert, G., Steinhäuser, C., & Bedner, P. (2020). Constitutive deletion of astrocytic connexins aggravates kainate-induced epilepsy. *Glia*, *68*, 2136–2147. https://doi.org/10.1002/glia.23832

Deshpande, T., Li, T., Herde, M. K., Becker, A., Vatter, H., Schwarz, M. K., Henneberger, C., Steinhäuser, C., & Bedner, P. (2017). Subcellular reorganization and altered phosphorylation of the astrocytic gap junction protein connexin43 in human and experimental temporal lobe epilepsy. *Glia*, *65*(11), 1809–1820. https://doi.org/10.1002/glia.23196

Devinsky, O., Vezzani, A., Najjar, S., De Lanerolle, N. C., & Rogawski, M. A. (2013). Glia and epilepsy: Excitability and inflammation. *Trends in Neurosciences*, *36*(3), 174–184. https://doi.org/10.1016/j.tins.2012.11.008

Di Nunzio, M., Di Sapia, R., Sorrentino, D., Kebede, V., Cerovic, M., & Gullotta, G. S., Bacigaluppi, M., Audinat, E., Marchi, N., Ravizza, T., Vezzani, A. (2021). Microglia proliferation plays distinct roles in acquired epilepsy depending on disease stages. *Epilepsia*, *62*(8), 1931–1945. https://doi.org/10.1111/epi.16956

Dissing-Olesen, L., LeDue, J. M., Rungta, R. L., Hefendehl, J. K., Choi, H. B., & MacVicar, B. A. (2014). Activation of neuronal NMDA receptors triggers transient ATP-mediated microglial process outgrowth. *Journal of Neuroscience*, *34*(32), 10511–10527. https://doi.org/10.1523/JNEUROSCI.0405-14.2014

Dong, Y., Fischer, R., Naudé, P. J. W., Maier, O., Nyakas, C., Duffey, M., Van der Zee, E. A., Dekens, D., Douwenga, W., Herrmann, A., Guenzi, E., Kontermann, R. E., Pfizenmaier, K., & Eisel, U. L. M. (2016). Essential protective role of tumor necrosis factor receptor 2 in neurodegeneration. *Proceedings of the National Academy of Sciences*, *113*(43), 12304–12309. https://doi.org/10.1073/pnas.1605195113

Escartin, C., Galea, E., Lakatos, A., O'Callaghan, J. P., Petzold, G. C., Serrano-Pozo, A., Steinhäuser, C., Volterra, A., Carmignoto, G., Agarwal, A., Allen, N. J., Araque, A., Barbeito, L., Barzilai, A., Bergles, D. E., Bonvento, G., Butt, A. M., Chen, W.-T., Cohen-Salmon, M., … Verkhratsky, A. (2021). Reactive astrocyte nomenclature, definitions, and future directions. *Nature Neuroscience*, *24*(3), 312–325. https://doi.org/10.1038/s41593-020-00783-4

Eyo, U. B., Peng, J., Swiatkowski, P., Mukherjee, A., Bispo, A., & Wu, L.-J. (2014). Neuronal hyperactivity recruits microglial processes via neuronal NMDA receptors and microglial P2Y12 receptors after status epilepticus. *Journal of Neuroscience*, *34*(32), 10528–10540. https://doi.org/10.1523/JNEUROSCI.0416-14.2014

Feng, L., Murugan, M., Bosco, D. B., Liu, Y., Peng, J., Worrell, G. A., Wang, H-.L., Ta, L. E., Richardson, J. R., Shen Y., Wu, L. (2019). Microglial proliferation and monocyte infiltration contribute to microgliosis following status epilepticus. *Glia*, *67*(8), 1434–1448. https://doi.org/10.1002/glia.23616

Fülle, L., Offermann, N., Hansen, J. N., Breithausen, B., Erazo, A. B., Schanz, O., Radau, L., Gondorf, F., Knöpper, K., Alferink, J., Abdullah, Z., Neumann, H., Weighardt, H., Henneberger, C., & Förster, I. (2018). CCL17 exerts a neuroimmune modulatory function and is expressed in hippocampal neurons. *Glia*, *66*(10), 2246–2261. https://doi.org/10.1002/glia.23507

Gao, L., Brenner, D., Llorens-Bobadilla, E., Saiz-Castro, G., Frank, T., Wieghofer, P., Hill, O., Thiemann, M., Karray, S., Prinz, M., Weishaupt, J. H., & Martin-Villalba, A. (2015). Infiltration of circulating myeloid cells through CD95L contributes to neurodegeneration in mice. *Journal of Experimental Medicine*, *212*(4), 469–480. https://doi.org/10.1084/jem.20132423

Gershen, L. D., Zanotti-Fregonara, P., Dustin, I. H., Liow, J.-S., Hirvonen, J., Kreisl, W. C., Jenko, K. J. Inati, S. K., Fujita, M., Morse, C. L., Brouwer, C., Hong, J. S., Pike, V. W., Zoghbi, S. S.,Innis, R. B., & Theodore, W. H. (2015). Neuroinflammation in temporal lobe epilepsy measured using positron emission tomographic imaging of translocator protein. *JAMA Neurology*, *72*(8), 882–888. https://doi.org/10.1001/jamaneurol.2015.0941

Goldmann, T., Wieghofer, P., Müller, P. F., Wolf, Y., Varol, D., Yona, S., Brendecke, S. M., Kierdorf, K., Staszewski, O., Datta, M., Luedde, T., Heikenwalder, M., Jung, S., & Prinz, M. (2013). A new type of microglia gene targeting shows TAK1 to be pivotal in CNS autoimmune inflammation. *Nature Neuroscience*, *16*(11), 1618–1626. https://doi.org/10.1038/nn.3531

Green, K. N., Crapser, J. D., & Hohsfield, L. A. (2020). To kill a microglia: A case for CSF1R inhibitors. *Trends in Immunology*, *41*(9), 771–784. https://doi.org/10.1016/j.it.2020.07.001

Grivennikov, S., Tumanov, A., Liepinsh, D., Kruglov, A., Marakusha, B., Shakhov, A., Murakami, T. Drutskaya, L. N., Förster, I., Clausen, B. E., Tessarollo, L., Ryffel, B., Kuprash, D. V., & Nedospasov, S. A. (2005). Distinct and nonredundant in vivo functions of TNF produced by T cells and macrophages/neutrophils protective and deleterious effects. *Immunity*, *22*(1), 93–104. https://doi.org/10.1016/S1074-7613(04)00379-6

Haghikia, A., Ladage, K., Lafênetre, P., Haghikia, A., Hinkerohe, D., Smikalla, D., Haase, C. G., Dermietzel, R., & Faustmann, P. M. (2008). Intracellular application of TNF-alpha impairs cell to cell communication via gap junctions in glioma cells. *Journal of Neuro-Oncology*, *86*(2), 143–152. https://doi.org/10.1007/s11060-007-9462-8

Hanisch, U.-K., & Kettenmann, H. (2007). Microglia: Active sensor and versatile effector cells in the normal and pathologic brain. *Nature Neuroscience*, *10*(11), 1387–1394. https://doi.org/10.1038/nn1997

Henning, L., Steinhäuser, C., & Bedner, P. (2021). Initiation of experimental temporal lobe epilepsy by early astrocyte uncoupling is independent of TGFβR1/ALK5 signaling. *Frontiers in Neurology*, *12*, 660591. https://doi.org/10.3389/fneur.2021.660591

Hiragi, T., Ikegaya, Y., & Koyama, R. (2018). Microglia after seizures and in epilepsy. *Cell*, *7*(4), 26. https://doi.org/10.3390/cells7040026

Jurga, A. M., Paleczna, M., & Kuter, K. Z. (2020). Overview of general and discriminating markers of differential microglia phenotypes. *Frontiers in Cellular Neuroscience*, *14*, 198. https://doi.org/10.3389/fncel.2020.00198

Kafitz, K. W., Meier, S. D., Stephan, J., & Rose, C. R. (2008). Developmental profile and properties of sulforhodamine 101—Labeled glial cells in acute brain slices of rat hippocampus. *Journal of Neuroscience Methods*, *169*(1), 84–92. https://doi.org/10.1016/j.jneumeth.2007.11.022

Karamita, M., Barnum, C., Möbius, W., Tansey, M. G., Szymkowski, D. E., Lassmann, H., & Probert, L. (2017). Therapeutic inhibition of soluble brain TNF promotes remyelination by increasing myelin phagocytosis by microglia. *JCI Insight*, *2*(8), e87455. https://doi.org/10.1172/jci.insight.87455

Käufer, C., Chhatbar, C., Bröer, S., Waltl, I., Ghita, L., Gerhauser, I., Kalinke, U., & Löscher, W. (2018). Chemokine receptors CCR2 and CX3CR1 regulate viral encephalitis-induced hippocampal damage but not seizures. *Proceedings of the National Academy of Sciences*, *115*(38), E8929–E8938. https://doi.org/10.1073/pnas.1806754115

Khan, D., Dupper, A., Deshpande, T., Graan, P. N. E. D., Steinhäuser, C., & Bedner, P. (2016). Experimental febrile seizures impair interastrocytic gap junction coupling in juvenile mice: Astrocyte uncoupling by febrile seizures. *Journal of Neuroscience Research*, *94*(9), 804–813. https://doi.org/10.1002/jnr.23726

Kim, S. Y., & Nair, M. G. (2019). Macrophages in wound healing: Activation and plasticity. *Immunology & Cell Biology*, *97*(3), 258–267. https://doi.org/10.1111/imcb.12236

Lehtimäki, K. A., Peltola, J., Koskikallio, E., Keränen, T., & Honkaniemi, J. (2003). Expression of cytokines and cytokine receptors in the rat brain after kainic acid-induced seizures. *Molecular Brain Research*, *110*(2), 253–260. https://doi.org/10.1016/S0169-328X(02)00654-X

Liddelow, S. A., Guttenplan, K. A., Clarke, L. E., Bennett, F. C., Bohlen, C. J., Schirmer, L., Bennett, M. L., Münch, A. E., Chung, W. S., Peterson, T. C., Wilton, D. K., Frouin, A., Napier, B. A., Panicker, N., Kumar, M., Buckwalter, M. S., Rowitch, D. H., Dawson, V. L., Dawson, T. M., … Barres, B. A. (2017). Neurotoxic reactive astrocytes are induced by activated microglia. *Nature*, *541*(7638), 481–487. https://doi.org/10.1038/nature21029

Liu, M., Jiang, L., Wen, M., Ke, Y., Tong, X., Huang, W., & Chen, R. (2020). Microglia depletion exacerbates acute seizures and hippocampal neuronal degeneration in mouse models of epilepsy. *American Journal of Physiology-Cell Physiology*, *319*(3), C605–C610. https://doi.org/10.1152/ajpcell.00205.2020

Löscher, W., Potschka, H., Sisodiya, S. M., & Vezzani, A. (2020). Drug resistance in epilepsy: Clinical impact, potential mechanisms, and new innovative treatment options. *Pharmacological Reviews*, *72*(3), 606–638. https://doi.org/10.1124/pr.120.019539

Même, W., Calvo, C., Froger, N., Ezan, P., Amigou, E., Koulakoff, A., & Giaume, C. (2006). Proinflammatory cytokines released from microglia inhibit gap junctions in astrocytes: Potentiation by β-amyloid. *The FASEB Journal*, *20*(3), 494–496. https://doi.org/10.1096/fj.05-4297fje

Merry, T. L., Brooks, A. E. S., Masson, S. W., Adams, S. E., Jaiswal, J. K., Jamieson, S. M. F., & Shepherd, P. R. (2020). The CSF1 receptor inhibitor pexidartinib (PLX3397) reduces tissue macrophage levels without

affecting glucose homeostasis in mice. *International Journal of Obesity*, *44*(1), 245–253. https://doi.org/10.1038/s41366-019-0355-7

Mirrione, M. M., Konomos, D. K., Gravanis, I., Dewey, S. L., Aguzzi, A., Heppner, F. L., & Tsirka, S. E. (2010). Microglial ablation and lipopolysaccharide preconditioning affects pilocarpine-induced seizures in mice. *Neurobiology of Disease*, *39*(1), 85–97. https://doi.org/10.1016/j.nbd.2010.04.001

Morin-Brureau, M., Milior, G., Royer, J., Chali, F., Le Duigou, C., Savary, E., Blugeon, C., Jourdren, L., Akbar, D., Dupont, S., Navarro, V., Baulac, M., Bielle, F., Mathon, B., Clemenceau, S., & Miles, R. (2018). Microglial phenotypes in the human epileptic temporal lobe. *Brain*, *141*(12), 3343–3360. https://doi.org/10.1093/brain/awy276

Nikolic, L., Shen, W., Nobili, P., Virenque, A., Ulmann, L., & Audinat, E. (2018). Blocking TNFα-driven astrocyte purinergic signaling restores normal synaptic activity during epileptogenesis. *Glia*, *66*(12), 2673–2683. https://doi.org/10.1002/glia.23519

Nolte, C., Matyash, M., Pivneva, T., Schipke, C. G., Ohlemeyer, C., Hanisch, U. K., Kirchhoff, F., & Kettenmann, H. (2001) GFAP promoter-controlled EGFP expressing transgenic mice: a tool to visualize astrocytes and astrogliosis in living brain tissue. *Glia 33*(1):72–86.

Onodera, M., Meyer, J., Furukawa, K., Hiraoka, Y., Aida, T., Tanaka, K., Rose, C. R., & Matsui, K. (2021). Exacerbation of epilepsy by astrocyte alkalization and gap junction uncoupling. *The Journal of Neuroscience*, *41*(10), 2106–2118. https://doi.org/10.1523/JNEUROSCI.2365-20.2020

Parkhurst, C. N., Yang, G., Ninan, I., Savas, J. N., Yates, J. R., Lafaille, J. J., Hempstead, B. L., Littman, D. R., & Gan, W.-B. (2013). Microglia promote learning-dependent synapse formation through brain-derived neurotrophic factor. *Cell*, *155*(7), 1596–1609. https://doi.org/10.1016/j.cell.2013.11.030

Pascual, O., Ben Achour, S., Rostaing, P., Triller, A., & Bessis, A. (2012). Microglia activation triggers astrocyte-mediated modulation of excitatory neurotransmission. *Proceedings of the National Academy of Sciences*, *109*(4), E197–E205. https://doi.org/10.1073/pnas.1111098109

Patel, D. C., Wallis, G., Dahle, E. J., McElroy, P. B., Thomson, K. E., Tesi, R. J., Szymkowski, D. E., West, P. J., Smeal, R. M., Patel, M., Fujinami, R. S., White, H. S., & Wilcox, K. S. (2017). Hippocampal TNFα signaling contributes to seizure generation in an infection-induced mouse model of limbic epilepsy. *Eneuro*, *4*(2). https://doi.org/10.1523/ENEURO.0105-17.2017

Probert, L., Akassoglou, K., Pasparakis, M., Kontogeorgost, G., & Kollias, G. (1995). Spontaneous inflammatory demyelinating disease in transgenic mice showing central nervous system-specific expression of tumor necrosis factor a. *Proceedings of the National Academy of Sciences*, *92*, 11294–11298.

Qin, C., Zhou, L.-Q., Ma, X.-T., Hu, Z.-W., Yang, S., Chen, M., Bosco, D. B., Wu, L.-J., & Tian, D.-S. (2019). Dual functions of microglia in ischemic stroke. *Neuroscience Bulletin*, *35*(5), 921–933. https://doi.org/10.1007/s12264-019-00388-3

R Core Team. (2021). R: A language and environment for statistical computing. 7 Feb 2022. https://www.r-project.org/.

Rana, A., & Musto, A. E. (2018). The role of inflammation in the development of epilepsy. *Journal of Neuroinflammation*, *15*(1), 144. https://doi.org/10.1186/s12974-018-1192-7

Riazi, K., Galic, M. A., Kuzmiski, J. B., Ho, W., Sharkey, K. A., & Pittman, Q. J. (2008). Microglial activation and TNF production mediate altered CNS excitability following peripheral inflammation. *Proceedings of the National Academy of Sciences*, *105*(44), 17151–17156. https://doi.org/10.1073/pnas.0806682105

Rice, R. A., Spangenberg, E. E., Yamate-Morgan, H., Lee, R. J., Arora, R. P. S., Hernandez, M. X., Tenner, A. J., West, B. L., & Green, K. N. (2015). Elimination of microglia improves functional outcomes following extensive neuronal loss in the hippocampus. *Journal of Neuroscience*, *35*(27), 9977–9989. https://doi.org/10.1523/JNEUROSCI.0336-15.2015

Rock, R. B., Gekker, G., Hu, S., Sheng, W. S., Cheeran, M., Lokensgard, J. R., & Peterson, P. K. (2004). Role of microglia in central nervous system infections. *Clinical Microbiology Reviews*, *17*(4), 942–964. https://doi.org/10.1128/CMR.17.4.942-964.2004

Rodgers, K. M., Hutchinson, M. R., Northcutt, A., Maier, S. F., Watkins, L. R., & Barth, D. S. (2009). The cortical innate immune response increases local neuronal excitability leading to seizures. *Brain*, *132*(9), 2478–2486. https://doi.org/10.1093/brain/awp177

Sanchez, J. M. S., DePaula-Silva, A. B., Doty, D. J., Truong, A., Libbey, J. E., & Fujinami, R. S. (2019). Microglial cell depletion is fatal with low level picornavirus infection of the central nervous system. *Journal of Neurovirology*, *25*(3), 415–421. https://doi.org/10.1007/s13365-019-00740-3

Sano, F., Shigetomi, E., Shinozaki, Y., Tsuzukiyama, H., Saito, K., Mikoshiba, K., Horiuchi, H., Cheung, D. L., Nabekura, J., Sugita, K., Aihara, M., & Koizumi, S. (2021). Reactive astrocyte-driven epileptogenesis is induced by microglia initially activated following status epilepticus. *JCI Insight*, *6*(9), e135391. https://doi.org/10.1172/jci.insight.135391

Schindelin, J., Arganda-Carreras, I., Frise, E., Kaynig, V., Longair, M., Pietzsch, T., Preibisch, S., Rueden, C., Saalfeld, S., Schmid, B., Tinevez, J.-Y., White, D. J., Hartenstein, V., Eliceiri, K., Tomancak, P., & Cardona, A. (2012). Fiji: An open-source platform for biological-image analysis. *Nature Methods*, *9*(7), 676–682. https://doi.org/10.1038/nmeth.2019

Seifert, G., Huttmann, K., Binder, D. K., Hartmann, C., Wyczynski, A., Neusch, C., & Steinhauser, C. (2009). Analysis of astroglial K+ channel expression in the developing hippocampus reveals a predominant role of the Kir4.1 subunit. *Journal of Neuroscience*, *29*(23), 7474–7488. https://doi.org/10.1523/JNEUROSCI.3790-08.2009

Tukey, J. W. (1977). *Exploratory data analysis*. Addison-Wesley Pub. Co. http://archive.org/details/exploratorydataa00tuke_0

Varvel, N. H., Neher, J. J., Bosch, A., Wang, W., Ransohoff, R. M., Miller, R. J., & Dingledine, R. (2016). Infiltrating monocytes promote brain inflammation and exacerbate neuronal damage after status epilepticus. *Proceedings of the National Academy of Sciences*, *113*(38), E5665–E5674. https://doi.org/10.1073/pnas.1604263113

Vezzani, A., Conti, M., Luigi, A. D., Ravizza, T., Moneta, D., Marchesi, F., & Simoni, M. G. D. (1999). Interleukin-1ß immunoreactivity and microglia are enhanced in the rat hippocampus by focal kainate application: Functional evidence for enhancement of electrographic seizures. *The Journal of Neuroscience*, *19*(12), 12–5065.

Vezzani, A., French, J., Bartfai, T., & Baram, T. Z. (2011). The role of inflammation in epilepsy. *Nature Reviews Neurology*, *7*(1), 31–40. https://doi.org/10.1038/nrneurol.2010.178

Vezzani, A., Moneta, D., Richichi, C., Aliprandi, M., Burrows, S. J., Ravizza, T., Perego, C., & De Simoni, M. G. (2002). Functional role of inflammatory cytokines and antiinflammatory molecules in seizures and epileptogenesis. *Epilepsia*, *43*, 30–35. https://doi.org/10.1046/j.1528-1157.43.s.5.14.x

Waltl, I., Käufer, C., Bröer, S., Chhatbar, C., Ghita, L., Gerhauser, I., Anjum, M., Kalinke, U., & Löscher, W. (2018). Macrophage depletion by liposome-encapsulated clodronate suppresses seizures but not hippocampal damage after acute viral encephalitis. *Neurobiology of Disease*, *110*, 192–205. https://doi.org/10.1016/j.nbd.2017.12.001

Waltl, I., Käufer, C., Gerhauser, I., Chhatbar, C., Ghita, L., Kalinke, U., & Löscher, W. (2018). Microglia have a protective role in viral encephalitis-induced seizure development and hippocampal damage. *Brain, Behavior, and Immunity*, *74*, 186–204. https://doi.org/10.1016/j.bbi.2018.09.006

Wang, N., Mi, X., Gao, B., Gu, J., Wang, W., Zhang, Y., & Wang, X. (2015). Minocycline inhibits brain inflammation and attenuates spontaneous recurrent seizures following pilocarpine-induced status epilepticus. *Neuroscience*, *287*, 144–156. https://doi.org/10.1016/j.neuroscience.2014.12.021

Weinberg, M. S., Blake, B. L., & McCown, T. J. (2013). Opposing actions of hippocampus TNFα receptors on limbic seizure susceptibility. *Experimental Neurology*, *247*, 429–437. https://doi.org/10.1016/j.expneurol.2013.01.011

Wobbrock, J. O., Findlater, L., Gergle, D., & Higgins, J. J. (2011). The aligned rank transform for nonparametric factorial analyses using only anova procedures. In *Proceedings of the SIGCHI conference on human factors in computing systems*, pp. 143–146. Vancouver, BC, Canada: ACM. https://doi.org/10.1145/1978942.1978963.

Wu, W., Li, Y., Wei, Y., Bosco, D. B., Xie, M., Zhao, M.-G., Richardson, J. R., & Wu, L.-J. (2020). Microglial depletion aggravates the severity of acute and chronic seizures in mice. *Brain, Behavior, and Immunity*, *89*, 245–255. https://doi.org/10.1016/j.bbi.2020.06.028

Wu, Z., Deshpande, T., Henning, L., Bedner, P., Seifert, G., & Steinhäuser, C. (2021). Cell death of hippocampal CA1 astrocytes during early epileptogenesis. *Epilepsia*, *62*(7), 1569–1583. https://doi.org/10.1111/epi.16910

Wyatt-Johnson, S. K., Herr, S. A., & Brewster, A. L. (2017). Status epilepticus triggers time-dependent alterations in microglia abundance and morphological phenotypes in the hippocampus. *Frontiers in Neurology*, *8*, 700. https://doi.org/10.3389/fneur.2017.00700

Yona, S., Kim, K.-W., Wolf, Y., Mildner, A., Varol, D., Breker, M., Strauss-Ayali,D.,Viukov,S.,Guilliams,M.,Misharin,A.,Hume,D.A.,Perlman,H.,Malissen, B., Zelzer, E., & Jung, S. (2013). Fate mapping reveals origins and dynamics of monocytes and tissue macrophages under homeostasis. *Immunity*, *38*(1), 79–91. https://doi.org/10.1016/j.immuni.2012.12.001

Zattoni, M., Mura, M. L., Deprez, F., Schwendener, R. A., Engelhardt, B., Frei, K., & Fritschy, J.-M. (2011). Brain infiltration of leukocytes contributes to the pathophysiology of temporal lobe epilepsy. *Journal of Neuroscience*, *31*(11), 4037–4050. https://doi.org/10.1523/JNEUROSCI.6210-10.2011

Zhao, X., Liao, Y., Morgan, S., Mathur, R., Feustel, P., Mazurkiewicz, J., Qian, J., Chang, J., Mathern, G. W., Adamo, M. A., Ritaccio, A. L., Gruenthal, M., Zhu, X., & Huang, Y. (2018). Noninflammatory changes of microglia are sufficient to cause epilepsy. *Cell Reports*, *22*(8), 2080–2093. https://doi.org/10.1016/j.celrep.2018.02.004

SUPPORTING INFORMATION

Additional supporting information can be found online in the Supporting Information section at the end of this article.

How to cite this article: Henning, L., Antony, H., Breuer, A., Müller, J., Seifert, G., Audinat, E., Singh, P., Brosseron, F., Heneka, M. T., Steinhäuser, C., & Bedner, P. (2023). Reactive microglia are the major source of tumor necrosis factor alpha and contribute to astrocyte dysfunction and acute seizures in experimental temporal lobe epilepsy. *Glia*, *71*(2), 168–186. https://doi.org/10.1002/glia.24265